Tectonics

RESEARCH ARTICLE
10.1029/2022TC007380

Thermo-Kinematic Evolution of the Eastern European Alps Along the TRANSALP Transect

Paul R. Eizenhöfer[1,2], Christoph Glotzbach[1], Jonas Kley[3], and Todd A. Ehlers[1,2]

[1]Department of Geosciences, Universität Tübingen, Tübingen, Germany, [2]Now at School of Geographical & Earth Sciences, University of Glasgow, Glasgow, Scotland, [3]Geoscience Centre, Universität Göttingen, Göttingen, Germany

Key Points:

- Exhumation in the eastern European Alps along TRANSALP is primarily driven by cooling through rock displacement along active faults
- The thermo-kinematic reconstruction emphasizes contrasts in the deformation north and south along TRANSALP since the Mid-Miocene
- In the absence of inter-plate rheological contrasts deformation patterns favor a reversal in subduction polarity since the Mid-Miocene

Supporting Information:

Supporting Information may be found in the online version of this article.

Correspondence to:

P. R. Eizenhöfer,
paul.eizenhoefer@glasgow.ac.uk

Citation:

Eizenhöfer, P. R., Glotzbach, C., Kley, J., & Ehlers, T. A. (2023). Thermo-kinematic evolution of the Eastern European Alps along the TRANSALP transect. *Tectonics*, *42*, e2022TC007380. https://doi.org/10.1029/2022TC007380

Received 6 MAY 2022
Accepted 23 MAR 2023

Author Contributions:

Conceptualization: Paul R. Eizenhöfer, Christoph Glotzbach, Jonas Kley
Formal analysis: Paul R. Eizenhöfer
Funding acquisition: Paul R. Eizenhöfer, Christoph Glotzbach, Jonas Kley, Todd A. Ehlers
Investigation: Paul R. Eizenhöfer, Jonas Kley
Methodology: Paul R. Eizenhöfer, Christoph Glotzbach
Project Administration: Paul R. Eizenhöfer, Christoph Glotzbach, Jonas Kley, Todd A. Ehlers
Resources: Christoph Glotzbach, Todd A. Ehlers

Abstract The eastern European Alps are shaped by the indentation of Adria into Europe. Recent tomography, depicting detached slab fragments, has been interpreted as evidence of continuous southward subduction of European lithosphere, contrary to an often-invoked subduction polarity reversal. Orogen-scale exhumation, driven by rock displacement along active faults, may reflect subduction polarity within the framework of doubly-vergent Coulomb wedge theory, provided the absence of rheological contrasts across the colliding plates. Low-temperature thermochronology can evaluate crustal cooling in response to changes in tectonic and erosional boundary conditions. This study investigates the consistency of observed crustal re-organization, exhumation, and mantle processes in the Eastern Alps. Thermo-kinematic forward models driven by reconstructions of crustal shortening along the TRANSALP geophysical transect were subjected to variations in shortening rates, thermophysical parameters, and topographic evolution, supplemented by new fission-track data. The thermo-kinematic models reproduce: (a) the orogen-scale structural geometry, (b) the distribution of thermochronometer ages, (c) observed time-temperature paths, and (f) the present-day surface heat flux. Results suggest that exhumation is driven by rock displacement along active faults without the need to involve mantle-driven buoyancy forces. Taken together, the results identify two possible scenarios: if the Tauern Ramp is a retro-thrust and the southward shift of deformation in the Southern Alps is a response to new Coulomb-wedge conditions, then our results support a Mid-Miocene reversal of the subduction polarity. Alternatively, crustal deformation does not reflect mantle processes entailing a high degree of inter-plate decoupling.

Plain Language Summary The convergence between the African and Eurasian plates created the European Alps. This process led to the Eurasian plate underlaying the African plate. It has been argued that this tectonic geometry changed, that is, Adria underlies Europe at present. Here we investigate whether changes in erosion and cooling of the crust over geologic time along a north-to-south profile in the Eastern Alps during the collision reflects deep seated mantle processes given the absence of rheological contrasts across the involved tectonic plates. New models for the structural and thermal evolution of the crust along the profile reproduce present-day structural and thermal observations. Model predictions are sensitive to heat production in the crust. Furthermore, these models indicate that cooling of the crust through erosion was primarily driven by the displacement of rocks toward the surface along active faults. Two possible tectonic scenarios are suggested: The pattern of fault activity during the collision is characteristic for an overlying European plate promoting that now the Adriatic plate lies under the European plate. If this is the case, this change in tectonic geometry likely occurred about 10–20 million years ago. Alternatively, crustal deformation does not reflect mantle processes because the interface between the two colliding plates is highly decoupled along the profile.

1. Introduction

Small convergent orogens such as Taiwan, the Southern Alps of New Zealand, the Pyrenees, and the Greater Caucasus have developed a doubly-vergent lithosphere geometry (e.g., Beaumont et al., 1996; Dahlen et al., 1984; Davis et al., 1983; Forte et al., 2014; Hardy et al., 2009; Naylor & Sinclair, 2007; Whipple & Meade, 2004; Willett et al., 1993). In these settings, the subducting plate (i.e., underlying the "pro-wedge") faces the oppositely dipping overriding plate (i.e., underlying the "retro-wedge"). The pro-wedge grows as new thrust sheets from the underlying plate are accreted while the deformation front rapidly propagates. In contrast, the retro-wedge is less active, and its deformation front only propagates outwards when thrust sheets from the overriding plate are incorporated (Naylor & Sinclair, 2007). The change in width of a doubly-vergent orogen is controlled by changes in either tectonic or climatic forcings, that is, in the ratio between accretionary flux to erosional efficacy

Software: Todd A. Ehlers
Validation: Paul R. Eizenhöfer, Christoph Glotzbach, Jonas Kley
Visualization: Paul R. Eizenhöfer, Jonas Kley
Writing – original draft: Paul R. Eizenhöfer
Writing – review & editing: Paul R. Eizenhöfer, Christoph Glotzbach, Jonas Kley, Todd A. Ehlers

(Stolar et al., 2006; Tomkin & Roe, 2007; Whipple & Meade, 2004; Willett & Brandon, 2002). Coulomb wedge theory applied to doubly-vergent orogens, enables the evaluation of upper lithospheric deformation relative to the thermophysical boundary conditions governing the colliding tectonic plates (e.g., Schlunegger & Willett, 1999). When orogen-scale changes in the above-described pattern of upper lithospheric deformation are observed during late-stage continental orogenesis, then the question remains unanswered if these are also reflective of changes in lower lithospheric processes such as a potential switch in the polarity of continental subduction.

Previous work highlights that the present-day European Alps are a type example of a double-vergent lithosphere geometry (Argand, 1916) and are a natural laboratory to test links between upper lithospheric deformation and lower lithospheric processes. The doubly-vergent geometry of the European Alps has been confirmed by deep seismic reflection measurements along the TRANSALP geophysical transect in the Eastern Alps (e.g., Lüschen et al., 2004, 2006). Since the Eocene to Oligocene, initiation of continent collisional processes between the subducting European and overriding Adriatic plates occurred in the Eastern Alps. As a consequence, the region east of the Giudicarie Line (following the definition for the Eastern Alps by Kissling & Schlunegger, 2018), grew laterally across-strike (e.g., Rosenberg et al., 2015). However, structural studies in the Northern Calcareous Alps (NCA) including the Helvetic Units and the Subalpine Molasse (e.g., Auer & Eisbacher, 2003; Ortner et al., 2015), the Tauern Window (e.g., Lammerer et al., 2008), and the Southern Alps (e.g., Castellarin et al., 2006) reveal an apparent, orogen-scale re-organization of fault activity in the Neogene. This re-organization resulted in minor post-Eocene fault activity in the NCA in contrast to Miocene in-sequence fault activation and present-day seismic activity in the Southern Alps (Anselmi et al., 2011; Caputo et al., 2010; Nussbaum, 2000; Schönborn, 1999; Serpelloni et al., 2016; Figure 1). Here we investigate the hypothesis that these orogen-scale changes in upper lithospheric deformation are indicative of a controversially discussed switch in the polarity of subduction in the Eastern Alps. Several studies (e.g., Eizenhöfer et al., 2021; Hetényi et al., 2018; Karousová et al., 2013; Kissling et al., 2006; Lippitsch, 2002; Lippitsch et al., 2003; Piromallo & Morelli, 2003) proposed a northwards dipping Adriatic slab, that is, a present-day subduction of the Adriatic plate beneath the European plate. Other studies have suggested the presence of a vertical to overturned delaminated European slab without the need for a subduction polarity reversal (e.g., Behm et al., 2007; Brückl et al., 2010; Castellarin et al., 2006; Dando et al., 2011; M. Handy et al., 2021; Kummerow et al., 2004; Mitterbauer et al., 2011). In addition, recent studies have suggested a slab break-off along the subducting European plate in the Eastern Alps at ~20 Ma, followed by surface uplift in the Northern Alpine Molasse Basin (M. R. Handy et al., 2015; Schlunegger & Kissling, 2022). Subsidence modeling in the Austrian part indicated that basin inversion occurred at 6–8 Ma (Genser et al., 2007) supported by thermochronological data from boreholes (Gusterhuber et al., 2012). This event may have facilitated the reorganization of the lower lithosphere during sustained continental convergence. Finally, tomographic images of the crust-mantle transition zone (~50–100 km) beneath central parts of the Eastern Alps, particularly beneath the Tauern Window, still do not provide a clear view on the interaction between the European and Adriatic plates at these depths. Hence, indirect approaches from the surface geology, such as the analysis of its thermal and structural archive, are still required to address this conundrum.

The application of low-temperature thermochronology in combination with Coulomb-wedge theory in doubly-vergent orogens offers one approach to evaluate lower lithospheric processes if certain boundary conditions are met. Low-temperature thermochronology studies of thrust belts enable the reconstruction of upper lithospheric processes based on reconstructed thermal histories from erosional exhumation induced rock cooling (e.g., Ehlers, 2005; Lock & Willett, 2008; McQuarrie & Ehlers, 2015, 2017). Records of hinterland cooling across the Eastern Alps can be used to test and further constrain physical parameters governing orogenesis along the TRANSALP transect through thermo-kinematic models. However, an orogen-scale interpretation of thermochronological data poses temporal and spatial challenges (e.g., variations in horizontal displacement, heterogenous thermophysical parameters, and changes in topographic evolution). This requires conducting orogen-scale thermo-kinematic models that enable the evaluation of kinematic, structural, thermophysical, and erosion scenarios and subsequent comparison with observational data (e.g., Barnhart et al., 2020a, 2020b). An additional complexity is added by the presence of Miocene lateral extrusion tectonics across the Eastern Alps. This resulted in a ~170 km lateral eastward motion of tectonic units north of the Periadriatic Fault (PF) (e.g., Frisch et al., 1998; Linzer et al., 2002; Ratschbacher, Frisch, et al., 1991; Ratschbacher, Merle, et al., 1991). However, lateral extrusion processes are difficult to reconcile with observed cooling ages because: (a) horizontal motion subparallel to the isotherms is an unlikely cause for vertical rock cooling, and (b) structures potentially driving vertical cooling such as the PF, the Inntal Fault and the Salzach-Ennstal-Mariazell-Puchberg fault (SEMP) are continuous

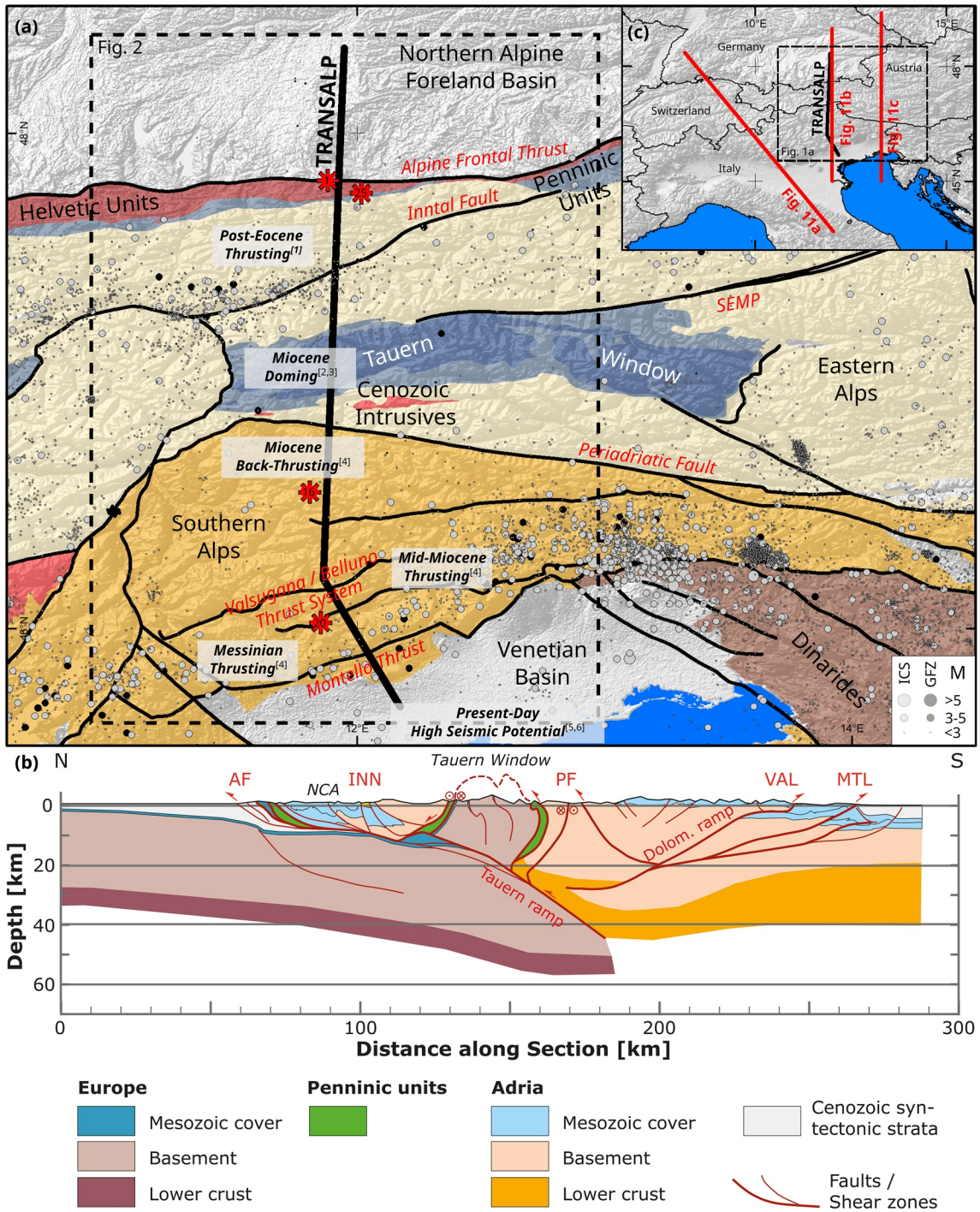

Figure 1. (a) Simplified geological map with significant faults and seismic events recorded by the International Seismological Center from 1950 to 2015 (ICS; Storchak et al., 2017) and the GEOFON Data Centre (1993) during 2011–2019. Gray boxes describe the reported timing and general characteristic of tectonic activity along TRANSALP since the Oligocene (numbers refer to references below). Red stars demarcate the location of new fission-track data, the number corresponding to the sample name (i.e., "Transalp-#"). (1) Auer and Eisbacher (2003), (2) Schmid et al. (2013), (3) Favaro et al. (2015), (4) Castellarin and Cantelli (2000), (5) Serpelloni et al. (2016), and (6) Moratto et al. (2019). SEMP, Salzach-Ennstal-Mariazell-Puchberg fault. (b) Geologic cross-section along the TRANSALP transect. The section is based on Lüschen et al. (2004) with modifications derived from Ortner et al. (2006). Geometry of the Tauern Ramp is from Lüschen et al. (2006). Northern Calcareous Alps (NCA) after Auer and Eisbacher (2003); near-surface southern Alps after Castellarin et al. (2006). Note, colors in legend refer to cross-section only. (c) Location of AlpArray *P*-wave travel time tomography profiles (Paffrath et al., 2021) shown in Figure 12. AF, Alpine Frontal Thrust; INN, Inntal Fault; PF, Periadriatic Fault; VAL, Valsugana/Belluno thrusts; MTL Montello thrust.

along-strike the Eastern Alps over large distances. Given this, we consider a simplified 2D thermal modeling approach suitable to improve our understanding of rock cooling in the region as a consequence of north-south convergence between Europe and Adria. We acknowledge that our estimates of the shortening required to induce the observed exhumation may be too low due to lateral extrusion, but they provide a starting point for identifying what processes could reproduce observed cooling ages. The application of Coulomb-wedge mechanics in doubly-vergent orogens requires the presence of horizontal forces (Willett et al., 1993) and the absence of strong rheological contrasts across the subducting and overriding plates (Vogt et al., 2017; Willingshofer et al., 2013). Horizontal forces have been present and were directed north-south in the eastern European Alps since at least ~20 Ma when the Southern Alps started recording active crustal deformation while the Alpine Frontal Thrust became largely inactive (e.g., Ortner et al., 2015; Schönborn, 1999; Ustaszewski et al., 2008). Prior to this time, the European plate subducted beneath the anticlockwise rotating, northward drifting Adriatic plate (e.g., Channell, 1992; Le Breton et al., 2021). In contrast, Kissling and Schlunegger (2018) argue that the Central Alps experienced slab roll-back due to an increase in slab load. Records of upper lithospheric deformation both, north and south of the PF (e.g., Castellarin et al., 2006; Lammerer et al., 2008; Rosenberg et al., 2018) indicate the absence of strong rheological contrasts in the Eastern Alps since the initiation of continental collisional processes.

In this study, we investigate the nature of doubly-vergent deformation in the upper lithosphere along the north-south oriented TRANSALP geophysical transect (Figure 1). We do this using a combination of structural and thermal numerical modeling. We evaluate the implications for deeper-seated tectonic processes within the framework of Coulomb-wedge theory in doubly-vergent orogens (e.g., Willett & Brandon, 2002; Willett et al., 1993). A suite of forward thermo-kinematic and erosion models is presented along the transect that encompasses the time since the onset of continental collision in the Eocene/Oligocene. In doing so, the first-order characteristics of the observed thermal record have been reconstructed and a strong sensitivity of thermochronometers to crustal deformation and volumetric heat production has been identified. Under the assumption that Coulomb-wedge criteria can be applied to post-20 Ma tectonic conditions, we assess the potential for a proposed Neogene continental subduction polarity reversal. Within this combined orogen-scale thermochronologic and geomechanical framework, the results of our study favor a continental subduction polarity reversal in the eastern European Alps along TRANSALP that may have occurred since the Mid-Miocene (Eizenhöfer et al., 2021). This subduction polarity reversal was potentially enabled by the continued indentation of Adria into Europe after European slab break-off at ~20 Ma (M. R. Handy et al., 2015; Schlunegger & Kissling, 2022).

2. Geological Background

After the closure of the Alpine Tethys (i.e., the Valais and Piemont oceans), the Adriatic plate overthrusted the southward subducting European plate leading to the formation of a doubly-vergent orogen geometry by the Late Eocene (e.g., Agard & Handy, 2021; M. R. Handy et al., 2015; Le Breton et al., 2021). During this time the pro- and retro-wedges were situated in the European and Adriatic plates, respectively. This lithosphere geometry is reflected in post-Eocene exhumation following thrust fault activity in the NCA north of the Inntal fault (e.g., Auer & Eisbacher, 2003) and the pre-Oligocene activity of back-thrust systems in the western Southern Alps ("Pre-Adamello Phase"; Castellarin et al., 2006). The onset of continental collision is thought to have resulted in tearing and break-off of the subducted Tethyan oceanic slab in the Early Oligocene, which provided space for asthenospheric upwelling, advection of heat, and the formation of intrusive bodies along the PF (Figure 1; von Blanckenburg & Davies, 1995). Since the Early Miocene (~20 Ma), fault activity has taken place primarily in the Southern Alps (Castellarin & Cantelli, 2000; Castellarin et al., 2006; Ustaszewski et al., 2008), while no significant fault activity has been detected along the Alpine Frontal Thrust (Auer & Eisbacher, 2003; Ustaszewski et al., 2008). At the same time, rapid exhumation is recorded across the Tauern Window as a result of north-south shortening due to Adriatic indentation and east-west extension accommodated along the Katschberg and Brenner normal faults (e.g., Bertrand et al., 2017; Favaro et al., 2015, 2017; Fügenschuh et al., 1997; Neubauer et al., 1999; Scharf et al., 2013; Wolff et al., 2021).

The thermochronological record reveals regions of active exhumation in the eastern European Alps since the Eocene/Oligocene beginning of continental collision (e.g., Fox et al., 2016; Rosenberg et al., 2018; Wölfler et al., 2012). Relating the crustal cooling histories north and south of the PF (i.e., the NCA including the Subalpine Molasse and Helvetic Units, the Tauern Window, and the Southern Alps) reveals links to changes in patterns of fault activity at the orogen-scale. Along TRANSALP, the timing and magnitudes of exhumation north of

10.1029/2022TC007380

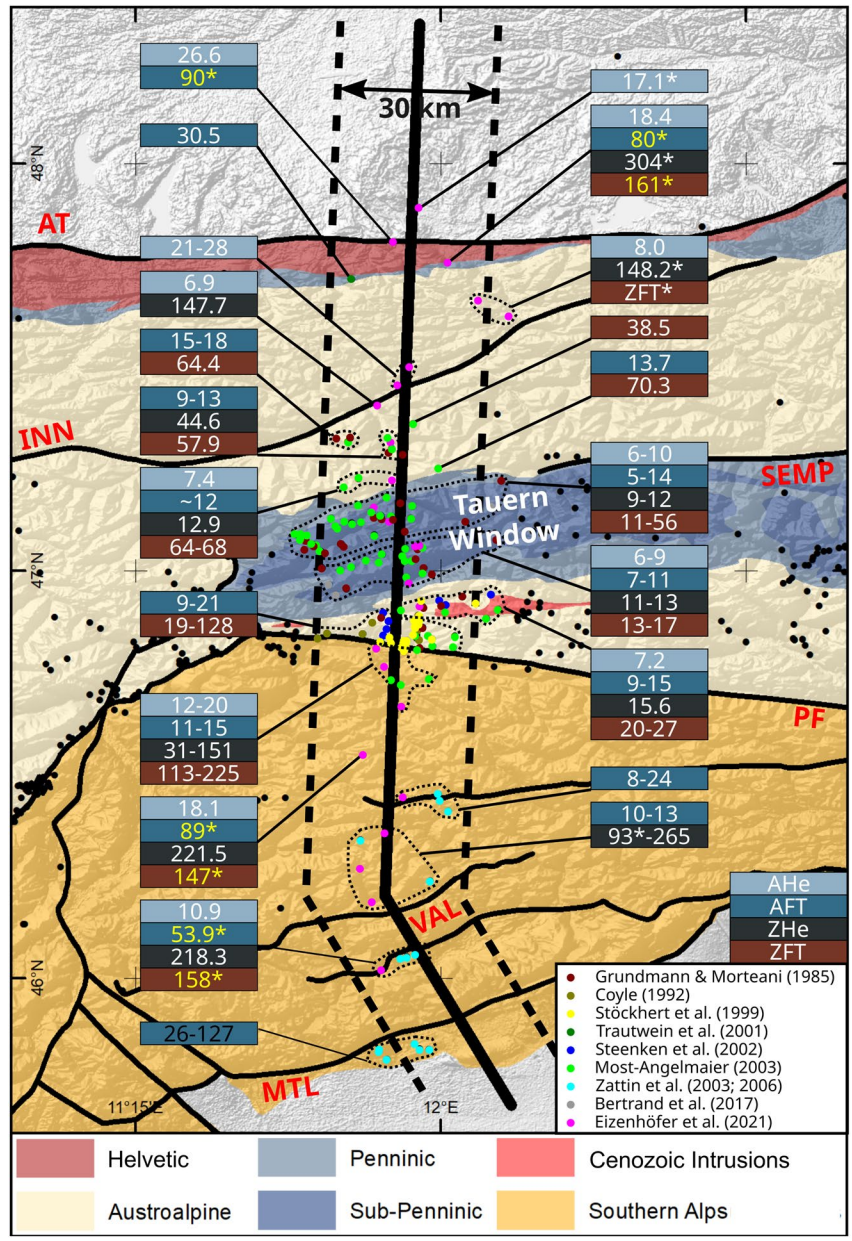

Figure 2. Simplified geological map (after Schmid et al., 2004) with published and new thermochronology data within a 30 km-wide swath along the TRANSALP geophysical transect (Lüschen et al., 2004). Black dots indicate locations of published, unspecified thermochronometer data outside of the swath, not considered in this study. Specified thermochronometer data from Grundmann and Morteani (1985), Coyle (1992), Stöckhert et al. (1999), Trautwein et al. (2001), Steenken et al. (2002), Most-Angelmaier (2003), Zattin et al. (2003, 2006), Bertrand et al. (2017), and Eizenhöfer et al. (2021). Age dates in yellow font are new. *mixed age (detrital, un-reset or partially reset). AT, Alpine Frontal Thrust; INN, Inntal fault; SEMP, Salzach-Ennstal-Mariazell-Puchberg fault; PF, Periadriatic Fault; VAL, Valsugana/Belluno thrust system; MTL, Montello thrust system.

the PF distinctly differ from that to the south (Figures 2 and 3a). Sedimentary rocks in the Northern Alpine Molasse Basin typically show un-reset, detrital thermochronology age distributions indicating that the basin has not been buried to great depths and that detritus is derived from local sources (e.g., Kuhlemann et al., 2006; this study). The Augenstein formation and Penninic units derived from early (~29–27 Ma) upright folding and doming in the area of the future Tauern Window have provided this material (Hülscher et al., 2019, 2021). Apatite (U-Th)/He (AHe) ages immediately north of the Alpine Frontal Thrust (Eizenhöfer et al., 2021) suggest that the present-day molasse surface was buried up to ~2 km depth in the Late Oligocene/Early Miocene (assuming

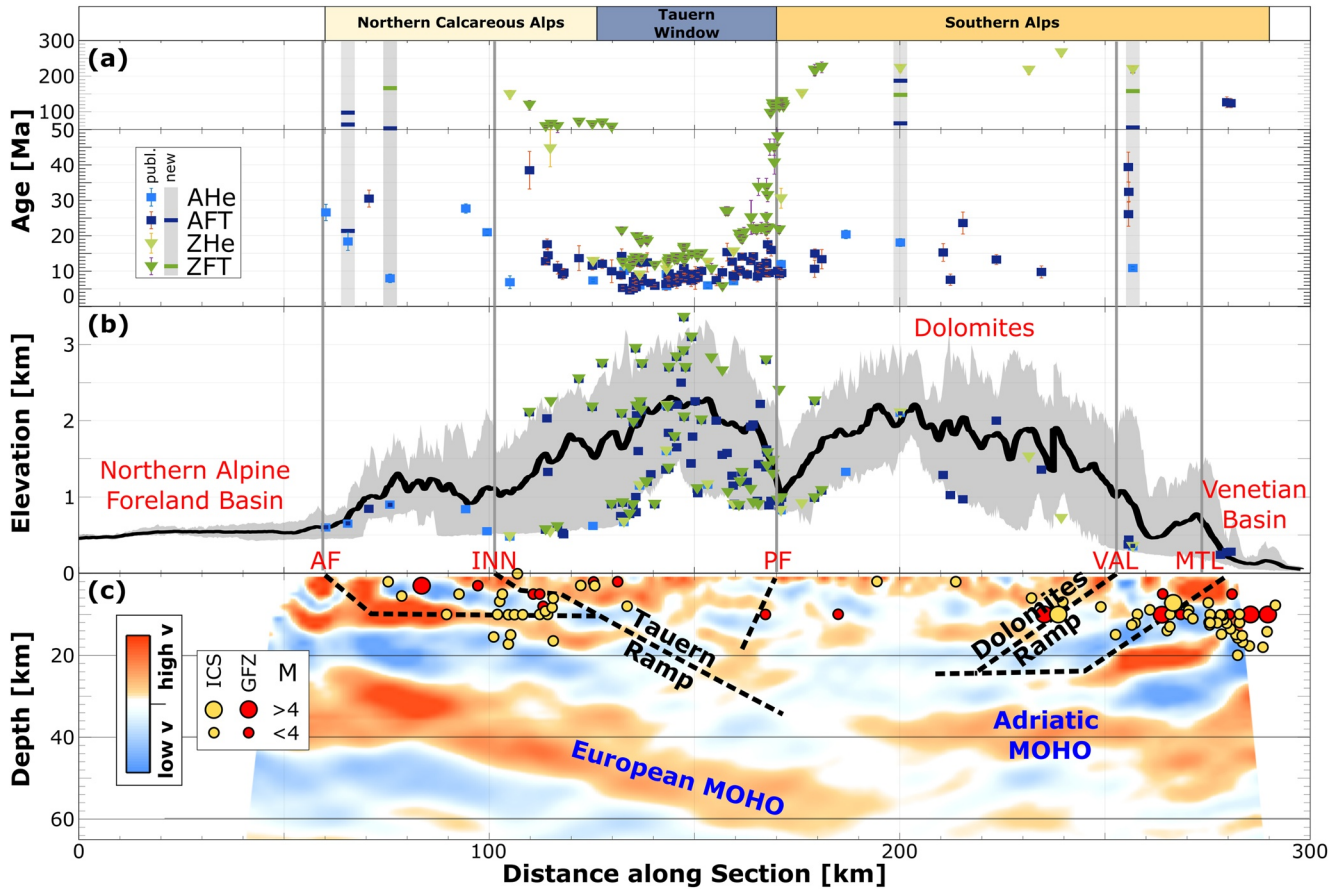

Figure 3. Thermochronologic, topographic, seismic, and structural data from a 30 km-wide swath along the TRANSALP geophysical transect (Lüschen et al., 2004). (a) Low-temperature thermochronologic ages (see Figure 2 for references); gray vertical bars depict the location of new un-reset fission-track data with thick horizontal bars demarking the central age of identified age populations. (b) Topographic profile (minimum, maximum, and mean elevation) with the locations of thermochronologic data with respect to elevation and distance along the transect, and (c) tomographic interpretation (Kummerow et al., 2004), recent seismicity (ICS, Storchak et al., 2017; GFZ, GEOFON Data Centre, 1993) and simplified structural geometry (Lüschen et al., 2004; this study). Modified after Eizenhöfer et al. (2021). AF, Alpine Frontal Thrust; INN, Inntal fault; PF, Periadriatic Fault; VAL, Valsugana/Belluno thrust system; MTL, Montello thrust system.

typical geothermal gradients). Thermochronologic data are sparse across the NCA between the Alpine Frontal Thrust and the Inntal fault due to the scarcity of apatite and zircon bearing lithologies. An Oligocene apatite fission-track age (Trautwein et al., 2001) combined with AHe ages in the range of 27.7–8.0 Ma and zircon (U-Th)/He (ZHe) ages >100 Ma (Eizenhöfer et al., 2021) indicate up to ~3 km of exhumation from the Oligocene to Late Miocene. Between the Inntal fault and the Tauern Window thermochronologic ages become successively younger southwards, ranging from ~7 Ma (AHe) over ~39–9 Ma (AFT) to ~148–13 Ma (ZHe; Grundmann & Morteani, 1985; Most-Angelmaier, 2003; Eizenhöfer et al., 2021). The Tauern Window is characteristic for its deep exhumation with thermochronologic ages below 10 Ma including the higher temperature systems (ZHe and zircon fission-track, ZFT; Bertrand et al., 2017; Eizenhöfer et al., 2021; Grundmann & Morteani, 1985; Most-Angelmaier, 2003). A minimum of ~7 km exhumation since the Mid-Miocene is interpreted as a response to 17 km displacement along the Tauern Ramp (Lammerer et al., 2008). Thermochronologic ages measured between the Tauern Window to the north and the PF to the south increase slightly to ages of ~6–9, ~7–21, ~11–13, and ~13–128 Ma for the AHe, AFT, ZHe, and ZFT systems, respectively (Coyle, 1992; Grundmann & Morteani, 1985; Most-Angelmaier, 2003; Steenken et al., 2002; Stöckhert et al., 1999). Hence, this region does show ages as young as those in the Tauern Window. However, higher-temperature cooling ages (e.g., the ZFT system) increase toward the PF, some being older than the initiation of continental collision (>30 Ma).

To investigate potential links to lower lithospheric processes along TRANSALP, it is crucial to precisely relate cooling patterns and the timing of faulting. Exhumation across the Southern Alps appears to reflect the sequential southward displacement of multiple southern Alpine thrust sheets (Figures 1–3a; Caputo et al., 2010; Castellarin

& Cantelli, 2000; Castellarin et al., 2006; Eizenhöfer et al., 2021; Schönborn, 1999): ZFT and ZHe ages across the PF southwards increase steeply, but monotonically, from ∼20 to >200 Ma (ZFT) and ∼15 to >200 Ma (ZHe) over a distance of <10 km, respectively (Eizenhöfer et al., 2021; Most-Angelmaier, 2003; Stöckhert et al., 1999). AFT and AHe ages generally increase immediately south of the PF, from ∼10 to 15–20 and ∼5 to ∼20 Ma, respectively (Eizenhöfer et al., 2021; Most-Angelmaier, 2003). The continuity of ages in these thermochronometer systems across the PF implies that only minor vertical displacement could have occurred since at least the Eocene/Oligocene due to the absence of any visible spatial offset of thermochronometer ages across the fault. This observation has been confirmed by recent studies along the Brenner Base Tunnel (Klotz et al., 2019). AFT ages across the Dolomites (Heberer et al., 2017; Zattin et al., 2006) range between ∼24 and ∼9 Ma. Their Alpine ages may reflect periods of active displacement along the Valsugana/Belluno thrust system and, hence, increased exhumation rates during the Mid-Miocene to Messinian (Castellarin & Cantelli, 2000). This process led to the exposure of the high-elevation Triassic basin platform (Schönborn, 1999). Integrated vitrinite reflectance and AFT analyses across the Dolomites further imply the residence of present-day bedrock at temperatures of ∼100°C immediately before the Alpine orogeny in the Cretaceous after prior Triassic burial (Zattin et al., 2003, 2006). This has been confirmed by recent thermal inversion models (Eizenhöfer et al., 2021). In comparison, older AFT ages >25 Ma (Zattin et al., 2003) and an AHe age of ∼10 Ma (Eizenhöfer et al., 2021) in the hanging wall of the Montello thrust system may imply only shallow exhumation of <4 km since the Messinian. This is consistent with a sequential southward migration of active thrusting (Castellarin & Cantelli, 2000). Hence, these thermochronometer ages may represent fast exhumation events in the past caused by rapid cooling below the AFT and AHe closure temperatures (∼80°C–100°C and ∼50°C–70°C, respectively; Ketcham et al., 2007; Flowers et al., 2009) at ∼25 and ∼10 Ma, respectively, followed by little erosion since then. However, seismic and kinematic studies indicate that the Montello thrust system continues to be active (e.g., Moratto et al., 2019; Serpelloni et al., 2016; Verwater et al., 2021). Present-day seismic activity in the Eastern Alps (GEOFON Data Centre, 1993; Storchak et al., 2017) is dominantly recorded across southern regions of the Southern Alps (Figure 1; Moratto et al., 2019; Serpelloni et al., 2016).

The geometry of the plate interface between Europe and Adria at ∼50–100 km depth still remains unclear. Surface and structural geometries along the Alpine Frontal Thrust, the NCA and the Southern Alps (e.g., Castellarin et al., 2006; Kilian et al., 2021; Linzer et al., 2002; Schönborn, 1999) suggest a doubly-vergent orogen geometry (Figure 3c) corroborated by the distribution of seismic activity (e.g., GEOFON Data Centre, 1993; Storchak et al., 2017) and reflection seismic imaging (Gebrande et al., 2002; Lüschen et al., 2004). Both, a southward European (Behm et al., 2007; Brückl et al., 2010; Castellarin et al., 2006; Dando et al., 2011; M. Handy et al., 2021; Kummerow et al., 2004; Mitterbauer et al., 2011) and northward Adriatic (Eizenhöfer et al., 2021; M. R. Handy et al., 2015; Kästle et al., 2020; Kissling et al., 2006; Pfiffner, 2005; Schmid et al., 2004) continental subduction have been suggested. However, the most recent studies (M. Handy et al., 2021; Paffrath et al., 2021) propose that the European slab has been detached at 25–10 Ma and consecutively overturned in the Eastern Alps, followed by continued southward subduction of the European lithosphere, in contrast to a previously debated northward polarity of subduction of Adriatic lithosphere further east in the Eastern Alps (Babuška et al., 1990; Hetényi et al., 2018; Karousová et al., 2013; Kästle et al., 2018, 2020; Koulakov et al., 2009; Lippitsch, 2002; Lippitsch et al., 2003; Zhao et al., 2016). Stratigraphic evidence in the Molasse basin further suggests a response to European slab break-off or delamination at ∼20 Ma (M. R. Handy et al., 2015; Schlunegger & Kissling, 2022).

3. Methodology

In this study, a 2D orogen-scale structural-kinematic and erosion model is applied for the evolution of the Eastern Alps along the TRANSALP geophysical transect (Figure 4). This is being done through a suite of thermal forward models (Figures 6–10; Figure S1 in Supporting Information S1) following the approach described in McQuarrie and Ehlers (2015, 2017). The models are supplemented by new AFT and ZFT thermochronology data (Figure 1; Figures S2 and S3 in Supporting Information S1; Table S1) with published, data-guided thermo-kinematic model validation (Figures 2 and 3).

3.1. Thermochronological Methods

The samples analyzed in this study originate from a field campaign that sampled systematically along the TRANSALP section to investigate its thermal evolution. A suite of (U-Th)/He apatite and zircon data derived

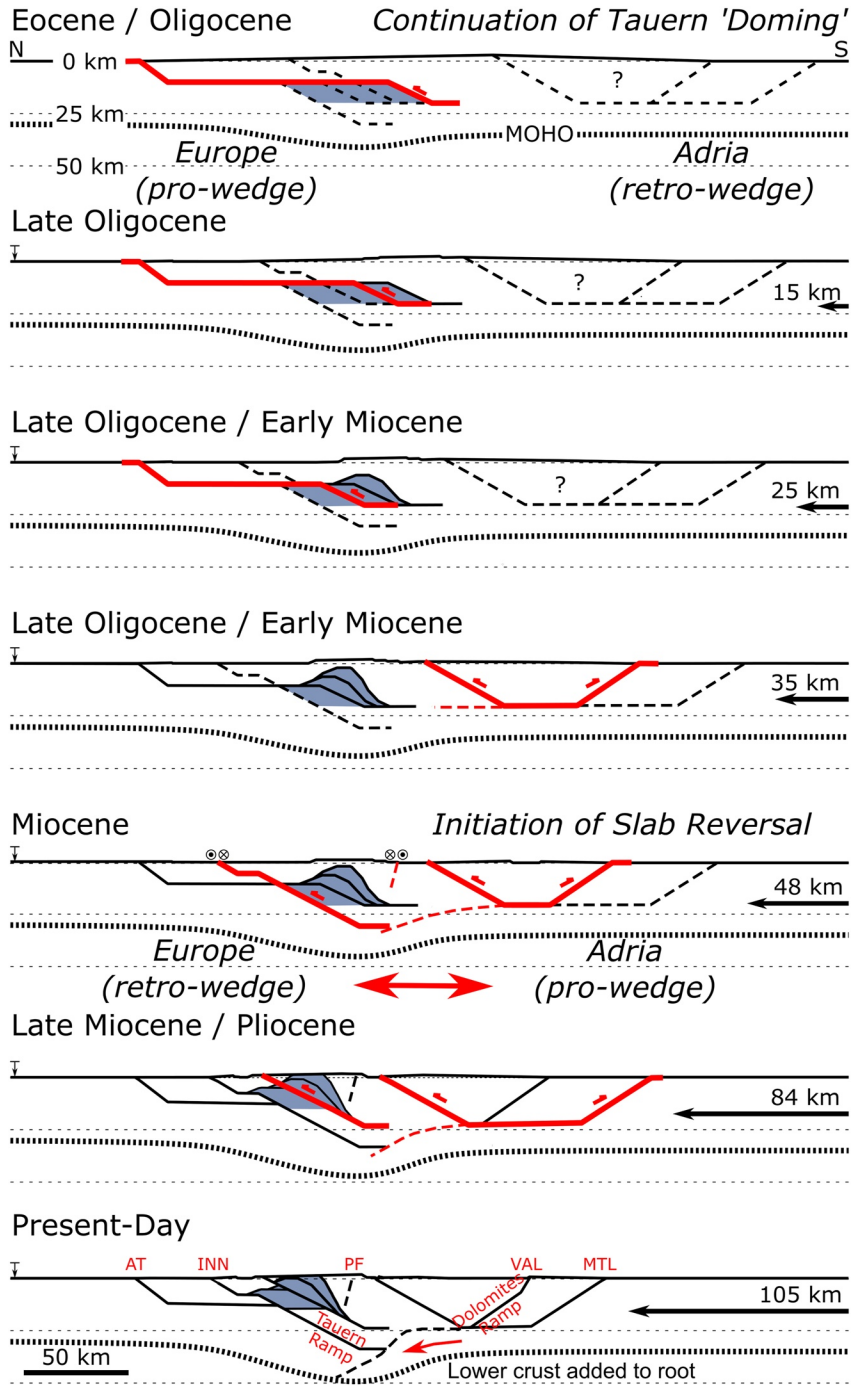

Figure 4. Proposed MOVE™ structural-kinematic evolution along TRANSALP (no vertical exaggeration, fixed Europe). The evolution of the Tauern Window since the Eocene/Oligocene is highlighted in gray-blue (earlier deformation not shown). AT, Alpine Frontal Thrust; INN, Inntal fault; PF, Periadriatic Fault; VAL, Valsugana/Belluno thrust system; MTL, Montello thrust system.

from this campaign has been presented in Eizenhöfer et al. (2021) (Figure 2). Four of these samples were selected for further AFT/ZFT analysis due to a scarcity of existing fission-track data at their sample location. The high thermochronology data density across the Tauern Window is sufficient to constrain its low-temperature (<250°C) history along TRANSALP in our thermo-kinematic models (see Section 3.3). North and south of the Tauern Window, however, data density is low in comparison due to non-suitable bedrock lithology. This

increases the degree of freedom and uncertainty for the subsurface structural-kinematic model in these regions (see Section 3.2). *Transalp-1* originates from clastics of the Subalpine Molasse south of the Alpine frontal thrust. *Transalp-25* was taken from the Upper Cretaceous "Reiselsberger Sandstone" of the Rhenodanubian Flysch. *Transalp-16* was extracted from sandstones of the Permian Bellerophon formation. *Transalp-20* is derived from sandstone clasts embedded within carbonaceous Triassic platform strata. The latter two are part of the post-Variscan, Permian-Mesozoic volcanic and sedimentary cover of the Southern Alps.

Apatite and zircon mineral extraction for the four samples followed standard techniques. Samples were crushed and sieved before undergoing magnetic and heavy liquid separation. Apatite and zircon separates were embedded in epoxy resin and Teflon™ sheets, respectively. The sample mounts were polished to expose internal surfaces at approximately half the grain size. Apatite mounts were etched in 5.5 mol HNO_3 for 20 s at 21°C (Donelick et al., 2005), and zircon mounts in a KOH:NaOH eutectic melt at 228°C until fission tracks were visible (Garver, 2003). We employed the mica external detector method (Gleadow, 1981) for all samples to determine the Uranium content. After neutron irradiation at the nuclear reactor BR1 in Mol/Belgium, micas were etched in 40% HF for 30 min at 21°C. Spontaneous and induced fission tracks were counted at 1,000× magnification on a Zeiss Axiolmager M2m microscope with AutoScan® soft- and hardware. Fission-track ages are calculated using the ζ age calibration method (Hurford & Green, 1983) using ζ-values of 249.9 ± 8.9 and 121.7 ± 4.1 for the AFT and ZFT systems (values for PRE), respectively. Data visualization and age mixture distribution analyses were aided by RadialPlotter (Vermeesch, 2009; Figures S1 and S2 in Supporting Information S1).

3.2. Structural-Kinematic Modeling

Reconstruction of rock trajectories along TRANSALP was performed in MOVE™ through orogen-scale upper lithospheric cross-section balancing in 2D (e.g., Dahlstrom, 1969). Our restored cross-section (Figure 4) attributes only minor vertical displacement to the PF given the absence of a break in the continuity of cooling ages across the fault (Figure 3a); this assumption has also been made in the "crocodile model" of the TRANSALP Working Group (Lüschen et al., 2004) and follows restorations by Lammerer et al. (2008). Since the onset of continental collision, crustal shortening has been accommodated across three tectonic units along the transect, that is, the NCA (including the Subalpine Molasse and Helvetic Units), the Tauern Window, and the Southern Alps. Across the NCA, Auer and Eisbacher (2003) describe some post-Eocene north-south contraction responsible for the truncation of older fold-thrust structures by post-Eocene deposits and north-directed thrusting within these sedimentary rocks. The exact amount of displacement, however, is unknown. Our reconstruction assumes 35 km of Early Miocene displacement accommodated along the Alpine Frontal Thrust. The displacement is led into a décollement beneath the NCA and linked to shortening during early duplexing across the Tauern region following reconstructions by Lammerer et al. (2008). The amount of shortening is consistent with a maximum of 50 km shortening across the Subalpine Molasse near the Rhine valley (decreasing to near zero toward Salzburg) during Miocene times (Ortner et al., 2015). This phase is followed by 17 km of blind-thrusting along the Tauern Ramp in the Mid- to Late Miocene and completed by 3 km of shortening along the Tauern north-boundary fault, a continuation of the SEMP further to the east (Figure 1; Table 2; Lammerer et al., 2008). Contrary to their work, the Tauern Ramp in our reconstruction leads into the Inntal fault (zone) following Ortner et al. (2006). Doming of the Tauern Window likely continues earlier cooling (e.g., Schneider et al., 2015) that is not explicitly modeled in our reconstruction but unlikely to have affected low-temperature thermochronometers (<250°C) such as the ones modeled in this study (the AHe, AFT, ZHe and ZFT systems). These are consistently reset across the Tauern Window as a result of later cooling. Across the Southern Alps, Castellarin and Cantelli (2000) suggest 16 km of shortening along the Valsugana/Belluno thrust system from the Mid-Miocene to Messinian, followed in-sequence by activity along the Montello thrust system accommodating 19 km of shortening since the Messinian. How both thrust systems lead into the deeper-seated Dolomites ramp and when active displacement took place along it remains uncertain (e.g., dashed lines in Schönborn, 1999). In our reconstruction the Dolomites ramp is primarily associated with the Valsugana/Belluno thrust system consistent with reconstructions by Castellarin and Cantelli (2000). Up to 15 km of displacement is accommodated mostly on north-verging structures as recorded in the metamorphic basement (phyllite belt) south of the PF and at the northern margin of the "Dolomites Synclinorium" (Castellarin et al., 2006). We have simplified these structures to a single back-thrust acting together with the Valsugana/Belluno and Montello thrust systems since the Mid-Miocene following reconstructions by Schönborn (1999). Similarly, the orogen-scale of our reconstruction prohibited a more detailed treatment of second-order, local structures described in detail for the NCA (includ-

Table 1
Thermophysical, Flexural and Erosional Numerical Model Parameter Ranges Including Model Dimensions

Property/Parameter	Model input value
Material properties	
Crustal volumetric heat production	1.0–6.0 μW/m^3
e-folding depth of crustal heat production	20 km
Thermal conductivity	3.0 W/mK
Specific heat capacity	800 J/kgK
Crustal density	2,650 kg/m^3
Mantle density	3,300 kg/m^3
Thermal properties	
Basal temperature	1,300°C
Surface temperature	10°C
Atmospheric lapse rate	6.5°C/km
Flexural parameters	
Effective elastic thickness	30 km
Erosional parameters	
Topographic growth to present-day	∼0–3 km
Angle of critical taper topography	0.5°–1.5°
Model dimensions	
Model base	110 km
Kinematic grid spacing	0.5 km
Model domain	550 × 110 × 2.5 km
Horizontal node spacing	0.5 km
Vertical node spacing	0.5 km

Note. Material parameters follow those determined independently by Tesauro et al. (2009) and Vosteen et al. (2003).

ing the Subalpine Molasse and Helvetic Units) and the Southern Alps (e.g., Auer & Eisbacher, 2003; Ortner et al., 2015; Schönborn, 1999). However, these are unlikely to have affected the regional orogen-scale cooling age pattern but may have caused local variations in cooling age patterns along TRANSALP and an underestimation of the total amount of shortening in the model. The total shortening in our structural-kinematic model (∼105 km) without east-west extrusion is similar to estimates by Frisch et al. (1998), 109–113 km, and Linzer et al. (2002), ∼95 km, but falls overall short relative to more recent estimates (e.g., 125 km when excluding 35 km of shortening along the Penninic Front; Rosenberg et al., 2021; 109–113 km of shortening north and >50 km south of the PF, respectively; Ustaszewski et al., 2008).

Cross-section balancing provides a tool to reconstruct the displacement of rock material over geologic time scales while maintaining equal rock area before and after deformation under a brittle regime and honoring observed geology. Maintenance of line lengths before and after a deformation step is ensured above active décollements, whereas beneath, it is assumed that crustal thickening occurs through unspecified "distributed deformation" reflecting a hybrid ductile/brittle state. This enabled us to implement a simplified evolution of the Mohorovičić discontinuity (Moho). Shortening above the décollement gives us a precise estimate of the area that needs to be accommodated between the décollement and the Moho eventually evolving into a "crustal bulge" beneath the Tauern Window. In this process, the Moho has been warped downward by the amount of material displaced between the décollement and the Moho with each deformation step (Figure 4). This approach assumes that crustal thickening is achieved through "distributed deformation" until the Moho reaches its present-day shape as determined by Kummerow et al. (2004). Their work has been selected because their receiver function analysis precisely follows the TRANSALP section line modeled in this study. Several studies have produced alternative Moho maps for the Eastern Alps (e.g., Behm et al., 2007; Brückl et al., 2010; Kind et al., 2021; Lippitsch, 2002; Lippitsch et al., 2003; Mitterbauer et al., 2011; Plomerová et al., 2022). However, a more detailed analysis of the thermophysical state of the crust-mantle interface is beyond the scope of this work. The primary objective of our approach is ensuring mass balance before and after deformation to reach a satisfactory solution for the present-day Moho. Implementing responses to deeper-seated geodynamic processes such as a rebound after potential slab delamination in the Eastern Alps (e.g., Schlunegger & Kissling, 2022) is beyond the framework of our model set up. If not constrained by literature sources, fault and décollement attitudes, geometries, and locations are reconstructed and placed as guided by structural trends suggested in existing orogen-scale cross-sections (Figure 1c; e.g., Lammerer et al., 2008; Lüschen et al., 2004).

Our structural-kinematic reconstructions are validated through the stepwise sequential deformation of the restored, undeformed section (Figure 4). In this forward kinematic modeling process, flexural and isostatic crustal responses to rock displacement and different modes of erosion were added (i.e., changing the angle of taper topography in individual model runs). Erosion is assumed to take place above a certain taper angle from the active deformation front for each modeled time step along both orogenic wedges (e.g., 1° in our preferred model). Flexural parameters and applied erosion models are given in Table 1. The selected flexural parameters are similar to those described in Andeweg and Cloetingh (1998) and Royden (1993). If the final, deformed state of the reconstruction matches the present-day surface geology, including known structural geometries such as the attitude of the Tauern Ramp (Lüschen et al., 2004), then the reconstruction is regarded as viable. Assigning time to each deformation step creates time-resolved rock displacement trajectories. Shortening rates (Table 2) closely follow Schmid et al. (1996) and are guided by changes in plate tectonic convergence rates inferred by Dewey et al. (1989), Müller et al. (2019), and Le Breton et al. (2021) for the Central and Eastern Alps. Rates by Ustaszewski et al. (2008) at an average of ∼10 mm/yr are slightly higher than these.

Table 2
Deformation Steps, Active Structures, Total Slip, Time of Activity, and Shortening Rates Applied to the Thermo-Kinematic Models

			This study		Schmid et al. (1996)[a]		Dewey et al. (1989)	
Step	Active structures	Total slip (km)	Time (Ma)	Shortening rate (mm/yr)	Time (Ma)	Shortening rate (mm/yr)	Time (Ma)	Shortening rate (mm/yr)
0	Alpine Frontal Thrust, Tauern Internal Deformation	0	24.8	4.5	29.7	4.5	21.3	9.4
1		15	21.4	4.5	26.3	4.5	19.7	9.4
2		25	19.2	4.5	24.1	4.5	18.7	9.4
3		35	17.0	4.5	21.9	4.5	17.6	9.4
4	Valsugana Thrust incl. Back-thrusting	48	12.7	3.0	19.0	4.5	13.3	3
5	Tauern Ramp, Valsugana Thrust incl. Back-thrust	81	5.3	4.5	8.0	3.0	5.6	4.3
6	Tauern north-boundary Fault, Montello Thrust	105	0.0	4.5	0.0	3.0	0.0	4.3

[a]Derived from the Central Alps/NFP-20E (~250 km east of TRANSALP).

3.3. Thermal Modeling and Thermochronologic Age Prediction

Viable structural-kinematic models are used to track rock displacement and simulate heat advection in a thermal model. The thermal model used is a University of Tübingen modified version of PECUBE ("Pecube-D"; Braun, 2003; McQuarrie & Ehlers, 2015, 2017; Whipp et al., 2009). "Pecube-D" is modified from the original version of PECUBE to include integration with the Move™ structural restoration software (McQuarrie & Ehlers, 2015, 2017), detrital thermochronometer age analysis (Whipp & Ehlers, 2019; Whipp et al., 2009), and inverse modeling of cooling ages for sample exhumation rates (Thiede & Ehlers, 2013). It solves the three-dimensional heat transport equation for user-defined topographies and surface boundary conditions. Age prediction algorithms for the (U-Th)/He and fission-track systems in apatite and zircon follow Farley (2000), Crowley (1991), Reiners et al. (2004), and Brandon et al. (1998). Input parameters for crustal volumetric heat production, thermal conductivity, and temperature at the base of the model match values described in Vosteen et al. (2003) and Tesauro et al. (2009) and are summarized in Table 1. However, heat production values determined for the Central and Western Alps through 1D thermal modeling are lower, in the range of 1.0–2.0 μWm^3 (Schlunegger & Willett, 1999).

The thermal models were validated using three data sets: first, the observed thermochronologic record (i.e., AHe, AFT, ZHe, and ZFT; Figures 2 and 3a); second, existing solutions of time-temperature (*t-T*) paths (Eizenhöfer et al., 2021; Zattin et al., 2006); and third, the surface heat flux as provided by the Global Heat Flow Database (www.heatflow.org; see Hurtig, 1995, for the European Alps; and references therein). Reduced χ^2-statistics (i.e., $\chi^2 = \sum_i \frac{(\text{age}_{i,\text{observed}} - \text{age}_{i,\text{model}})^2}{\text{variance}_{i,\text{observed}}}$) are used to evaluate the goodness-of-fit between predicted and observed

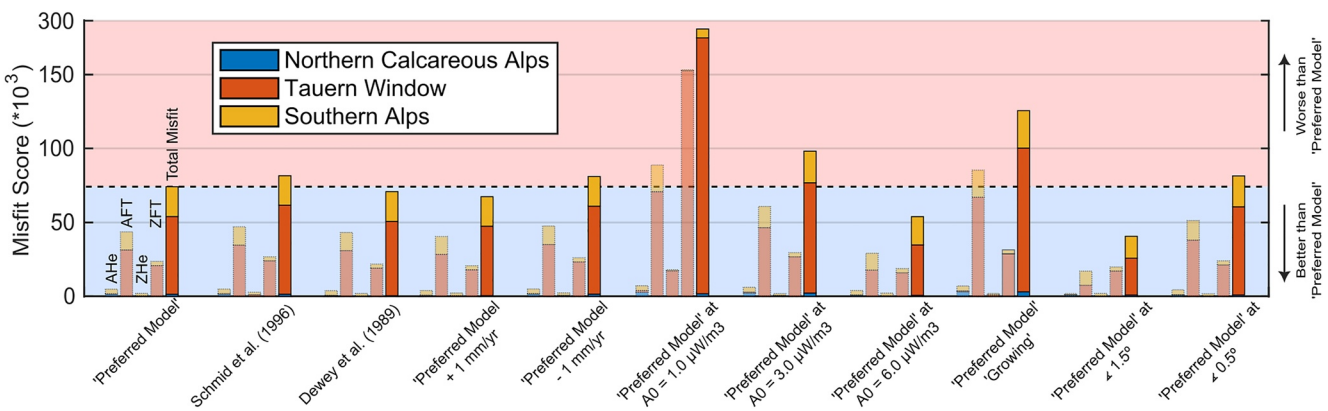

Figure 5. Summary of reduced χ^2-statistics ("Misfit Score") for thermo-kinematic models based on input kinematics shown in Figure 4. The fifth column from the left for each set depicts the total misfit score including color-coded contributions from the three major tectonic units. The four columns to the left in each set show the individual contributions of the modeled thermochronometers to the total misfit score. Note, the misfit score is strongly influenced by data modeled and observed in the Tauern Window due to its high data density. In contrast, the statistical contribution in the Northern Calcareous Alps is minor due to its lack of observed data.

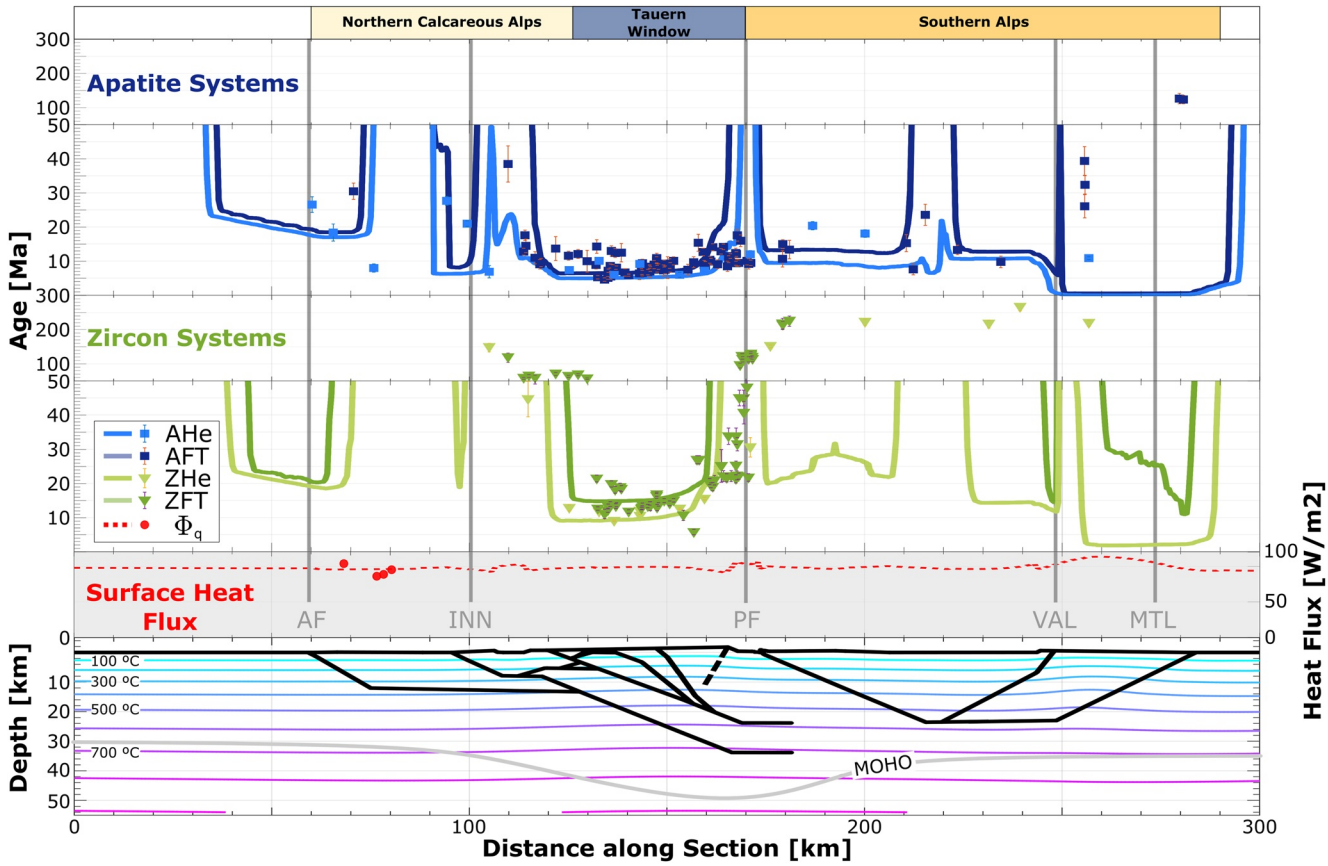

Figure 6. "Preferred" forward thermo-kinematic model along the TRANSALP transect. Predicted and measured present-day thermochronologic ages (solid lines and data points, respectively) for the apatite (AHe, AFT) and zircon (ZHe, ZFT) systems are shown in the top two panels, predicted and observed heat flux in the third (dashed line and data points, respectively), shaded panel, the modeled thermal field based on the kinematic sequence in Figure 4 including modeled MOHO and tapered model topography on the bottom panel (no vertical exaggeration). AHe and ZHe, apatite and zircon (U-Th)/He; AFT and ZFT, apatite and zircon fission-track; Φ_q, heat flux [W/m^2]. AT, Alpine Frontal Thrust; INN, Inntal fault; PF, Periadriatic Fault; VAL, Valsugana/Belluno thrust system; MTL, Montello thrust system.

thermochronometer ages (Figure 5; Table 3 and Table S3). Given the high variability of thermochronometer ages, heterogenous observed data density along the transect, and the forward modeling nature limiting the total number of models that can be statistically evaluated, the χ^2-values (used here as $\chi^2_{score} = \chi^2 \times 10^{-3}$) enable ranking the performance of individual model runs, that is, low χ^2-values indicate a better goodness-of-fit than high values. Integrating complex structural kinematics with a thermal model currently only allows a forward modeling approach. Nevertheless, input parameters are within observed value ranges, and both, structural-kinematic and thermal models, are independently validated through comparison with observed data. Hence, the thermal and structural-kinematic models are viable if they can predict the general trend of structural geometry, observed thermochronometer ages, sample *t-T* paths, and present-day heat flux.

4. Results

4.1. New Thermochronology Data

The distribution of published thermochronology ages along TRANSALP reflects a distinct exhumation pattern that has been defined by continental collision since the Eocene/Oligocene (e.g., Eizenhöfer et al., 2021; Figure 3). Our analysis of four new samples is consistent with this observation. New fission-track data from two samples of Miocene clastic strata of the Subalpine Molasse and Upper Cretaceous Rhenodanubian Flysch confirm that exhumation north of the NCA did not reach levels that reset the AFT or ZFT systems during Neogene continental collision processes. Therefore, the Miocene sample (*Transalp-1*) records its detrital origin whereas the Upper Cretaceous sample (*Transalp-25*) may have recorded a Cretaceous/Paleogene cooling event (Figure 1, Figures S1

and S2 in Supporting Information S1; Tables S1 and S2). AFT results for each sample fail the χ^2-test indicating the presence of multiple age populations. Mixture distribution analyses suggest the presence of two to four age populations centered in the Carboniferous, Cretaceous, Eocene, and Miocene. The oldest AFT age population may have been derived from Variscan sources in the Central Alps west of the Giudicarie Line where such cooling ages have been reported (e.g., Garzanti & Malusà, 2008). The youngest age population (~21.3 Ma) implies that source material may be derived from the orogenic interior during the Alpine orogeny, for example, the Central Alps, where the Lepontine Dome was exposed during that time (Boston et al., 2017; Kuhlemann et al., 2006; Schlunegger & Willett, 1999) or the Tauern Window post-20 Ma (e.g., Hülscher et al., 2019, 2021; Schlunegger & Kissling, 2022). ZFT data from *Transalp-25* failed the χ^2-test. Mixture distribution analysis (Figure S2 in Supporting Information S1) remains inconclusive due to the wide range, or perhaps a small number, of single grains analyzed, but suggests the presence of at least one age population centered in the Jurassic (~167.0 Ma). This suggests that the Cretaceous/Paleogene cooling event did not affect the ZFT system. Hence, ZFT ages in this sample may reflect their detrital source because of the Cretaceous depositional age of the sample.

New fission-track data from two locations in the Southern Alps comprising Permian and Triassic clastic strata may have recorded a Cretaceous/Paleogene cooling event but have otherwise not been affected by later continental collisional processes (Figure 1, Figures S1 and S2 in Supporting Information S1; Tables S1 and S2). χ^2-tests performed on the AFT data failed to indicate the presence of multiple age populations. Mixture distribution analysis suggests minor Jurassic (~187 Ma) and dominant Late Cretaceous/Early Palaeogene (~68.5 and ~53.3 Ma) age populations. New ZFT data for these two samples do not fail the χ^2-test indicating no significant statistical variability (assuming a 0.05 significance criterion) and, hence, the presence of a single age population. Given the samples in the Southern Alps are of Permian and Triassic origin, they have likely experienced a lower Jurassic cooling event (i.e., ~149 and ~158 Ma). Some bedrock ZFT data a few kilometers south of the PF show similar age ranges (e.g., Most-Angelmaier, 2003; Stöckhert et al., 1999) consistent with our new ZFT data. Since the new thermochronological data have not been reset during Alpine orogeny, it does not hold direct information on the thermal history of orogeny. However, it can be used to constrain the maximum temperatures reached and related exhumation.

4.2. Thermo-Kinematic Models

In the following, forward thermo-kinematic model solutions along the TRANSALP transect are presented (Figures 5–10). Timing of fault activity, thermal boundary conditions, and the evolution of topography are the primary controls on the cooling history of a region. To assess their sensitivity along TRANSALP, (a) a meaningful set of shortening rates was applied (Table 2; Figure 8), (b) varied crustal volumetric heat production values from $A_0 = 1.0$ to 6.0 μW/m^3 were implemented (Figure 9), and (c) different scenarios for the topographic evolution were investigated (Figure 10). These sensitivity analyses guided model calibrations to find an acceptable model ("Preferred Model"; Section 3.3) that adopts realistic input parameters and is ultimately validated against independent observations (i.e., orogen-scale structural geometry, heat flux, thermochronology ages, and *t*-*T*-paths). However, trade-offs among the input parameters prohibit precise quantification because alternative combinations of input parameters may yield similar, non-unique modeling results.

Predicted age variabilities depend strongly on the thermochronometer system and the *t*-*T* path a sample experienced (Figure 11). Temperature deviations between different models (e.g., of ~20°C) have a minor effect on the resulting thermochronologic age in rapidly cooled regions (e.g., the Tauern Window) compared to areas that dwelled for extended periods at temperatures around the closure temperature (e.g., in the partial annealing zone of the AFT/ZFT systems). The latter case may reflect either tectonic inactivity and/or horizontal displacement along low-angle décollements during tectonic activity (e.g., in the NCA and the Southern Alps). The resulting age variabilities along TRANSALP are ~1–2 Myr in the Tauern Window (rapid cooling) in comparison to ~20 Myr for the NCA and the Southern Alps (slow cooling). Not all thermochronometers of a single sample are affected in the same way by variations in thermal boundary conditions. This is the case if the sample-specific exhumation path is complex (e.g., a combination of horizontal displacement followed by vertical rock uplift). For example, periods of fast cooling in the Southern Alps affect the AHe and AFT systems. In contrast, the higher temperature ZHe and ZFT systems are more sensitive to the prolonged dwelling at higher temperatures. Hence, they exhibit a higher predicted age variability when thermal boundary conditions and/or timing of fault activity change. Prevailing uncertainties in the timing of fault activity and the thermal boundary conditions will reduce the predictive power

and precision of individual thermo-kinematic models. Instead, assessing a range of thermo-kinematic models and input parameters reflecting these uncertainties may be more appropriate (Figures 8–11).

4.2.1. Preferred Thermo-Kinematic Model

First the preferred forward thermo-kinematic model is introduced to facilitate the presentation of our results and sensitivity analyses. This model reproduces the observed geology, thermochronologic and thermal heat flux data along the TRANSALP transect well (Table 1) while adopting reasonable kinematic, thermal and topographic input parameters. The kinematic sequence is described in Section 3.2 and shown in Figure 4; shortening rates of 4.5 mm/yr until the Mid-Miocene, followed by 3.0 mm/yr until the Pliocene and 4.5 mm/yr until the present day produced a sufficiently small statistical misfit in comparison to alternative rates (Table 2). As expected, these values are well below plate tectonic convergence rates that are in the range of 10 mm/yr (Dewey et al., 1989; Le Breton et al., 2021; Müller et al., 2019; Ustaszewski et al., 2008). They are overall higher than the ones suggested by Schmid et al. (1996) which is consistent with their data being obtained from the Central Alps. Due to the counterclockwise rotation of Adria, north-south shortening rates along the TRANSALP transect would increase eastwards. However, even though our chosen shortening rates (and the resulting predicted cooling ages) reproduce the observed thermal record, independent verification is required to confirm these since our predicted cooling ages show little sensitivity to variations in shortening rates (Figure 8, Sections 4.2.2 and 5.1). Crustal volumetric heat production is set at 4.5 $\mu W/m^3$. A tapered topography at 1° is assumed along both orogenic wedges which approximates the present-day topographic gradient across the north and south of the Eastern Alps along TRANSALP (Figure 3b). All other input parameters are the same in the models and are provided in Table 1. Despite the physical heterogeneities observed along the TRANSALP transect, the input parameters represent a "good" average within documented parameter ranges (Tesauro et al., 2009; Vosteen et al., 2003).

The pattern of predicted thermochronologic ages and *t-T* paths (Figures 6 and 7) is closely tied to the sequential activity of faults along the TRANSALP transect (Figure S1 in Supporting Information S1). Compared to the other models, the preferred model statistically performs better than most others ($\chi^2_{score} = 74.00$; Figure 5, Table 3 and Table S1). Goodness-of-fit improves by adopting a 1.5° tapered topography ($\chi^2_{score} = 40.63$), higher Miocene shortening rates ($\chi^2_{score} = 70.70$ and $\chi^2_{score} = 67.26$), and high crustal heat production values ($\chi^2_{score} = 54.22$). However, these models may be considered less geologically viable for the following reasons: (a) the present-day topography is closer to an average tapered topography of 1°; (b) Miocene shortening rates >4.5 mm/yr at an average plate tectonic convergence rate of 5.8 mm/yr (Müller et al., 2019) would imply that most of the plate tectonic shortening had been accommodated through crustal deformation; (c) high crustal heat production values only apply across the Tauern Window (Vosteen et al., 2003); and (d) high thermochronologic data density across the Tauern Window biases the statistical evaluation because the NCA (including the Subalpine Molasse and Helvetic Units) and the Southern Alps contribute only to a minor degree to the overall misfit-score (Figure 5).

Statistical fits vary concerning the tectonic unit (i.e., the Tauern Window, the NCA including the Subalpine Molasse and Helvetic Units, and the Southern Alps) and the thermochronometer system (AHe, AFT, ZHe, and ZFT; Figure 5, Table S3). Modeled Eocene/Oligocene doming of the Tauern region led to a complete reset of all thermochronometer systems (AHe, $\chi^2_{score,\ AHe} = 0.25$; AFT, $\chi^2_{score} = 31.36$; ZHe, $\chi^2_{score} = 0.18$; ZFT, $\chi^2_{score} = 20.82$). The ZHe and ZFT systems preserved some record of this event, whereas the AHe and AFT systems have been overprinted by later activity along the Tauern Ramp. Mid-Miocene activity of the Tauern Ramp leads to a complete reset in the AFT and AHe systems and a partial reset in the ZHe system across the Tauern region and south of the Inntal fault north of the Tauern Window. Displacement along the Tauern north-boundary fault has a negligible influence on the predicted age distribution pattern causing a slight broadening of reset ZFT ages above the Tauern Window south of the Tauern north-boundary fault. Increasing thermal heat production to 6.0 $\mu W/m^3$ improves the data fit relative to the preferred model for all except for the ZHe system (AHe, $\chi^2_{score} = 0.20$; AFT, $\chi^2_{score} = 17.69$; ZHe, $\chi^2_{score} = 0.32$; ZFT, $\chi^2_{score} = 15.91$). Increasing the topographic taper to 1.5° produces better statistical results relative to the preferred model for the AFT, ZHe, and ZFT systems (AHe, $\chi^2_{score} = 0.29$; AFT, $\chi^2_{score} = 7.49$; ZHe, $\chi^2_{score} = 0.15$; ZFT, $\chi^2_{score} = 17.11$). Marginal improvements relative to the preferred model are achieved for all thermochronometer systems with high Miocene shortening rates that adopt high plate tectonic shortening rates proposed by Dewey et al. (1989) (AHe, $\chi^2_{score} = 0.22$; AFT, $\chi^2_{score} = 30.95$; ZHe, $\chi^2_{score} = 0.13$; ZFT, $\chi^2_{score} = 19.03$). In the NCA (including the Subalpine Molasse and Helvetic Units), Early Miocene activity along the Alpine Frontal Thrust reset all four thermochronometer systems in our preferred model (AHe, $\chi^2_{score} = 1.38$; AFT, $\chi^2_{score} = 0.01$; ZHe, $\chi^2_{score} =$ n/a; ZFT, $\chi^2_{score} =$ n/a). The data fit

relative to the preferred model for the AHe system across the NCA improves at higher Miocene shortening rates (χ^2_{score} = 0.39 and 0.42), higher heat production values (χ^2_{score} = 0.66), and a higher topographic taper of 1.5° (χ^2_{score} = 0.83). In contrast, the data fit for the AFT systems remains unaffected due to a general lack of observed AFT data (χ^2_{score} = 0.01 and 0.02, χ^2_{score} = 0.01, and χ^2_{score} = 0.01, for higher shortening rates, heat production and topographic taper, respectively). In the Southern Alps Miocene fault activity along the Valsugana/Belluno thrust system, including back thrusting initially resets the ZHe, AFT, and AHe systems in our preferred model. The ZFT system resets later during the post-Miocene activity of the Montello thrust system (AHe, χ^2_{score} = 3.20; AFT, χ^2_{score} = 12.28; ZHe, χ^2_{score} = 1.74; ZFT, χ^2_{score} = 2.78). Higher heat production produces better statistical fits in the lower temperature AHe and AFT systems relative to the preferred model (AHe, χ^2_{score} = 3.05; AFT, χ^2_{score} = 11.48; ZHe, χ^2_{score} = 2.13; ZFT, χ^2_{score} = 18.72). In contrast, lower heat production values are statistically

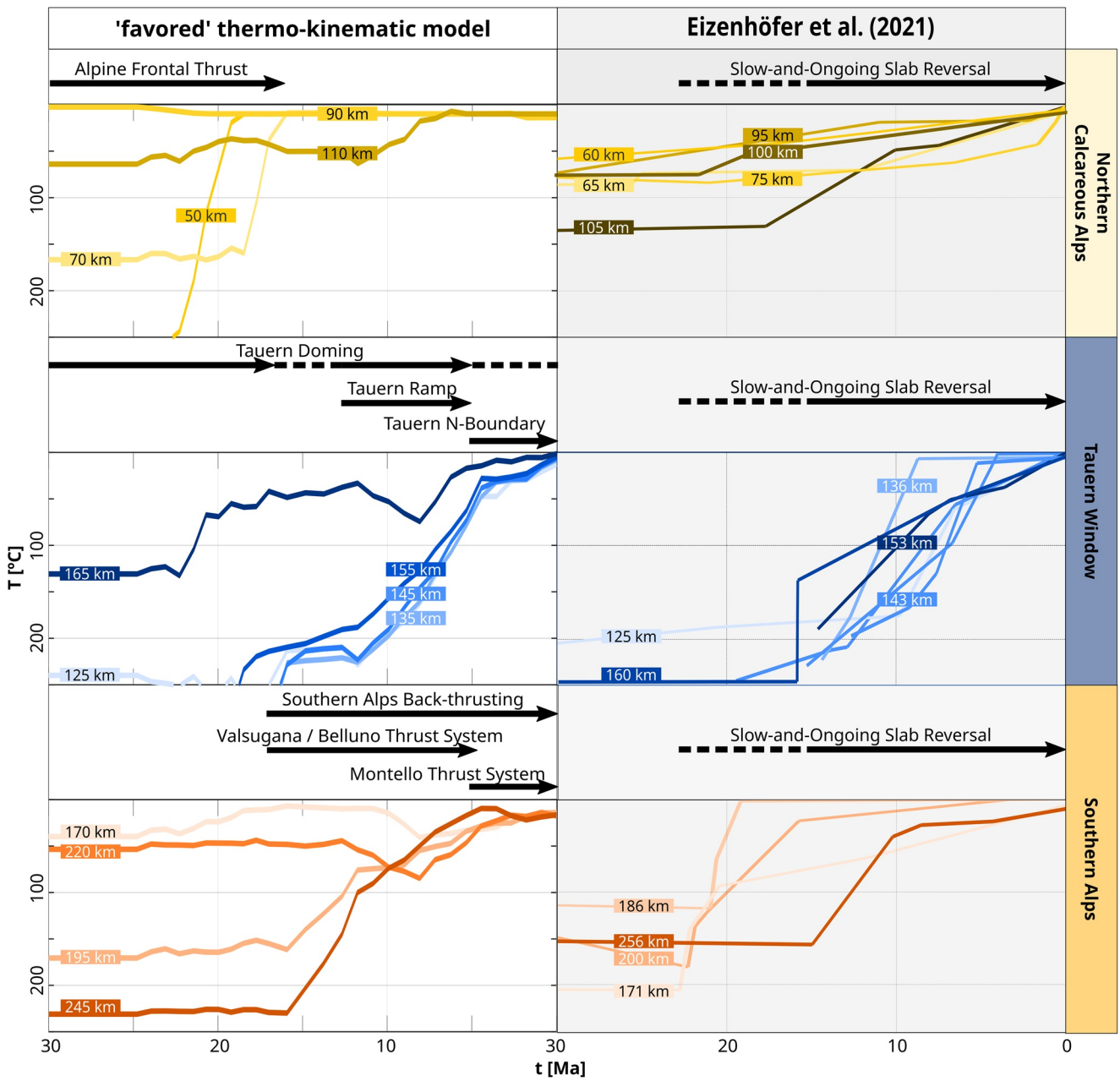

Figure 7. Comparison of time-temperature-paths extracted from the preferred thermo-kinematic model in this study (left column) with best-fit thermal inverse modeling results from Eizenhöfer et al. (2021; right column) along the TRANSALP transect. Horizontal arrows indicate the timing of major tectonic events above each suite of *t*-*T* paths. Distances are given with respect to the northern end of the transect.

preferred for the higher temperature ZHe and ZFT systems relative to the preferred model (AHe, χ^2_{score} = 3.27; AFT, χ^2_{score} = 14.17; ZHe, χ^2_{score} = 1.16; ZFT, χ^2_{score} = 2.78). Statistical fits improve at a 1.5° tapered topography except for the ZHe system relative to the preferred model (AHe, χ^2_{score} = 0.71; AFT, χ^2_{score} = 9.53; ZHe, χ^2_{score} = 1.77; ZFT, χ^2_{score} = 2.75). In both cases, across the NCA and the Southern Alps, low observed data density and more complex structural-kinematic models minimize the value of applying reduced χ^2-statistics in assessing model performance, in contrast to the Tauern Window.

t-T paths extracted from the preferred thermo-kinematic model enable insights into the cooling history along TRANSALP and add another validation level (Figure 7). Figure 7 demonstrates the resemblance of *t-T* paths derived from our preferred thermo-kinematic model with independently determined data-driven thermal inversion *t-T*-path solutions (Eizenhöfer et al., 2021). The NCA (including the Subalpine Molasse and Helvetic Units) generally show minor to no cooling south of the Inntal fault. Since the continental collision, modeled temperatures south of the Alpine Frontal Thrust never exceeded ~100°C. The *t-T* paths south of the Alpine Frontal Thrust at <60 km distance along the section, show high temperatures (>100°C) early in the model. Approaching the Tauern Window, samples become more affected by Tauern Ramp activity due to the structural relationship between the Tauern Ramp and the Inntal fault. Sample points across the Tauern Window consistently show steep cooling rates from at least ~200°C in the Mid-Miocene to <50ºC in the Late Miocene, reflecting displacement along the Tauern Ramp. Samples between the PF and the Tauern Window experienced cooling from <200°C, where the Tauern Ramp flattens out southwards in the model. Cooling paths across the Southern Alps are dominated by moderate to fast cooling during 20–10 Ma from temperatures exceeding ~150°C to <100ºC after a period of slight cooling at 30–20 Ma. The results are consistent with relative isotherm-parallel displacement followed by activity along the individual thrust systems in our model. The overall resemblance of the *t-T*-paths between existing thermal model inversions and those derived from our forward models underlines that sample-specific *t-T* paths result from the structural evolution along TRANSALP. Notably, slow cooling does not necessarily reflect "tectonic quiescence." It could also represent isotherm-parallel displacement during an active tectonic phase (e.g., samples moving along a flat detachment before getting exhumed above a ramp). In the model, samples in the Southern Alps moved ~30 km horizontally before being uplifted while active exhumation took place across the Tauern Window and continental collision was underway (Figures 4 and 7).

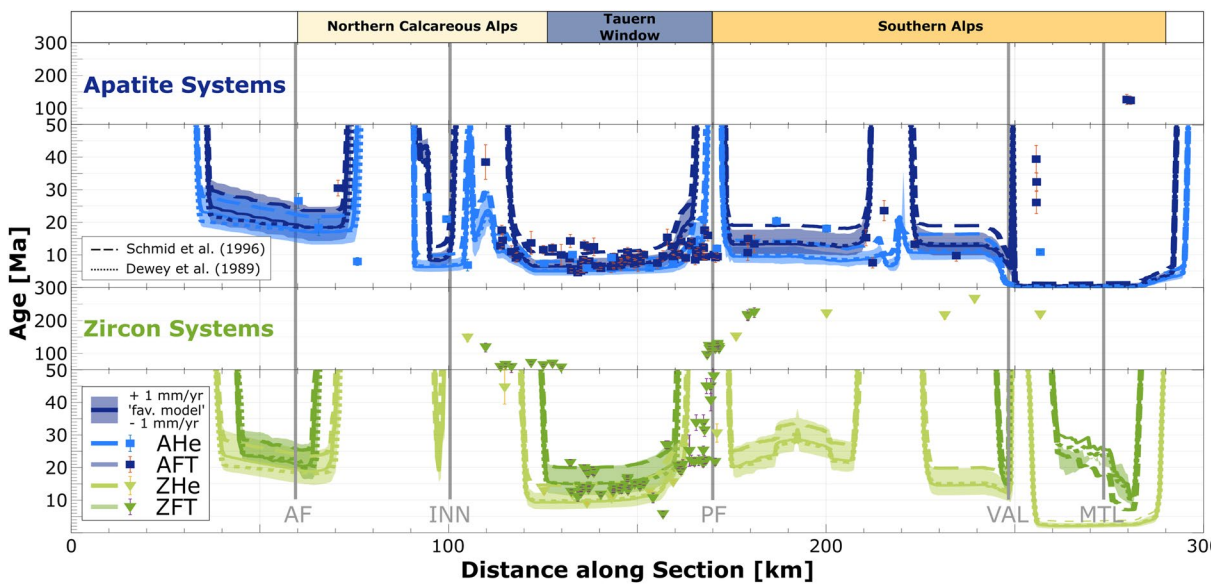

Figure 8. Thermo-kinematic model sensitivity under variable shortening rates. Preferred model ("fav. model") shortening rates are at 4.5 mm/yr (24.8–12.7 Ma), 3.0 mm/yr (12.7–9.0 Ma) and 4.5 mm/yr (9.0 Ma to present-day). AT, Alpine Frontal Thrust; INN, Inntal fault; PF, Periadriatic Fault; VAL, Valsugana/Belluno thrust system; MTL, Montello thrust system.

4.2.2. Effect of Shortening Rates on Thermochronometer Ages

We applied two additional sets of convergence rates to our thermo-kinematic model (Table 2). One suite of models assumed a shortening rate of 4.5 mm/yr until the Mid-Miocene, slowing to 3.0 mm/yr until today (Schmid et al., 1996). Another simulation adopts high plate tectonic shortening rates of 9.4 mm/yr until the Mid-Miocene, followed by a short period of 3.0 mm/yr in the Mid-Miocene before shortening rates increase to 4.3 mm/yr until the present-day (Dewey et al., 1989). As expected, varying convergence rates does not affect the overall distribution and pattern of predicted thermochronologic ages. Instead, predicted ages generally increase with lower shortening rates and vice versa (Figure 8). Predicted ages following convergence rates by Schmid et al. (1996) are generally ~5 Myr older than those of the preferred model and produce a greater statistical misfit (χ^2_{score} = 81.44; Table 3). This result is not unexpected because the applied shortening rates have been established in the Central Alps and are in considerable proximity to TRANSALP where shortening rates would be slightly higher as a consequence of the counter-clockwise rotation of Adria. Age predictions following plate tectonic convergence rates by Dewey et al. (1989) are marginally different from the preferred model and produce slightly improved statistical fits (χ^2_{score} = 70.70). However, lateral extrusion tectonics in the Eastern Alps (e.g., Ratschbacher, Frisch, et al., 1991; Ratschbacher, Merle, et al., 1991) requires that not all plate tectonic convergence could have been accommodated by thrust/reverse faulting along the TRANSALP transect.

In addition, we increased and reduced convergence rates by 1 mm/yr in our preferred model to assess the ensuing variability of predicted ages. Our results indicate that variability differs for individual thermochronologic systems and locations. ZFT ages across the Tauern Window vary by more than 10 Myr, whereas ZHe, AFT, and AHe ages are more confined and vary by not more than ~5 Myr. Across the NCA, predicted ZHe, AFT, and AHe ages may change by ~10 Myr, but variability is more confined (<5 Myr) toward the Tauern Window. Age variations across the Southern Alps increase slightly for higher temperature systems from ~5 Myr in the AHe system to <10 Myr in the AFT and ZHe systems. Predicted AFT and AHe ages appear primarily unaffected by variations in shortening rates across the Montello thrust system with variations of ~1–2 Myr only. Increasing shortening rates improves the statistical fit (χ^2_{score} = 67.26; Table 3). However, such high shortening rates (i.e., 4.5 mm/yr), are approaching average plate tectonic convergence rates of 5.8 mm/yr (Dewey et al., 1989; Müller et al., 2019). Hence, these must be treated with caution due to the presence of lateral extrusion tectonics.

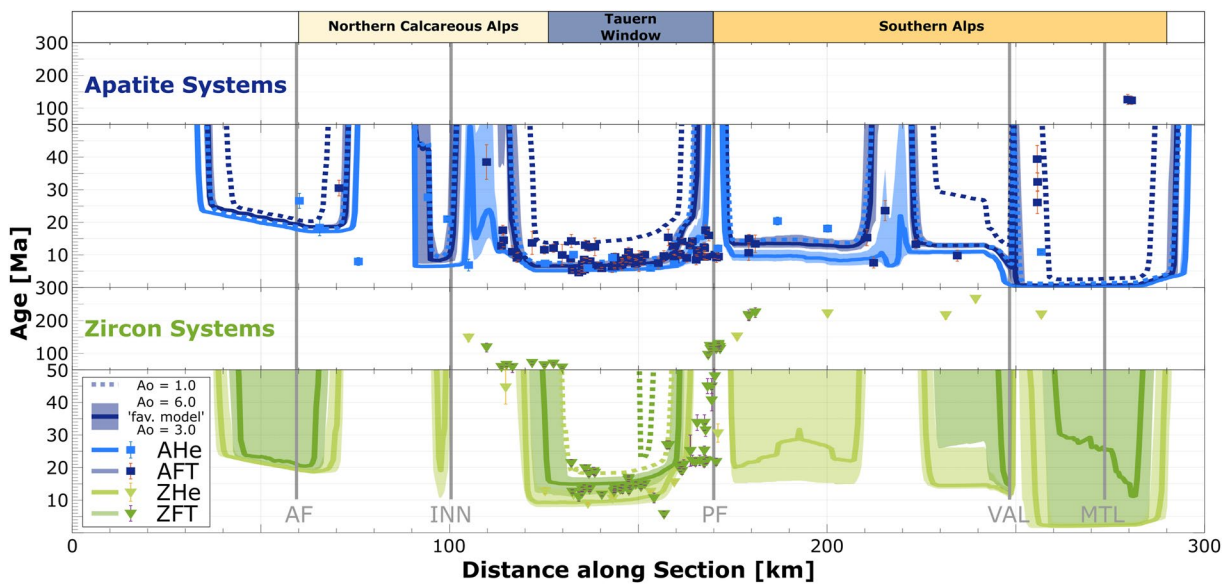

Figure 9. Thermo-kinematic model sensitivity under variable crustal volumetric heat production at constant thermal conductivity (3.0 W/mK). Preferred model ("fav. model") is at A_0 = 4.5 μW/m^3. AT, Alpine Frontal Thrust; INN, Inntal fault; PF, Periadriatic Fault; VAL, Valsugana/Belluno thrust system; MTL, Montello thrust system.

4.2.3. Effect of Thermophysical Model Parameters on Thermochronometer Ages

Here sensitivity analyses on variations in heat production for our preferred model are presented to evaluate the role of thermophysical parameters on predicted thermochronology ages. Vosteen et al. (2003) have shown that crustal heat production values along TRANSALP are near A_0 = 1 μW/m^3 in the foreland basins and may reach up to A_0 = 6 μW/m^3 in the middle to lower crustal materials exposed across the Tauern Window. Higher values improve the data fit across the Tauern Window relative to the preferred model (AHe, χ^2_{score} = 0.20; AFT, χ^2_{score} = 17.69; ZHe, χ^2_{score} = 0.32; ZFT, χ^2_{score} = 15.91; Table S1). However, the misfit statistics are biased concerning model performance along the entire transect due to the high data density across the Tauern Window. There, crustal volumetric heat production values are higher than across the NCA (including the Subalpine Molasse and Helvetic Units) and the Southern Alps. Our experiments indicate that the highest temperature thermochronometric systems (ZHe and ZFT) are the most sensitive to variations in crustal heat production (Figure 9). Small changes in crustal heat production result in significant changes in age prediction. Across the Tauern Window, the AHe and AFT systems show an age variability of ∼1–2 Myr. The ZHe and ZFT systems have a slightly increased variability of up to ∼5 Myr. In the Southern Alps, the higher temperature systems (ZFT and ZHe) show very high age variations of at least ∼20 Myr, except for the ZHe system across the Montello thrust system. The AFT and AHe systems produce variations in ages of up to ∼5 Myr. The NCA show a similar age variability concerning temperature as the Southern Alps, where ZHe, AFT, and AHe ages only vary by ∼1–2 Myr in contrast to the ZFT system with considerable age variations. Assuming a heat production value of 1.0 μW/mK, representative of foreland basin sedimentary material, resetting higher temperature systems takes place only above the Tauern and Dolomites ramps. Nevertheless, statistical fits relative to the preferred model do not improve with lower crustal heat production values across the NCA (AHe, χ^2_{score} = 2.15 and 2.65; AFT, χ^2_{score} = 0.01 and 0.25; ZHe, χ^2_{score} = n/a; ZFT, χ^2_{score} = n/a; for A_0 = 3.0 μW/m^3 and 1.0 μW/m^3, respectively) or the Southern Alps (AHe, χ^2_{score} = 3.27 and 3.27; AFT, χ^2_{score} = 14.17 and 18.06; ZHe, χ^2_{score} = 1.16 and 0.74; ZFT, χ^2_{score} = 2.78 and 2.81, for A_0 = 3.0 and 1.0 μW/m^3, respectively), probably due to low observed data density.

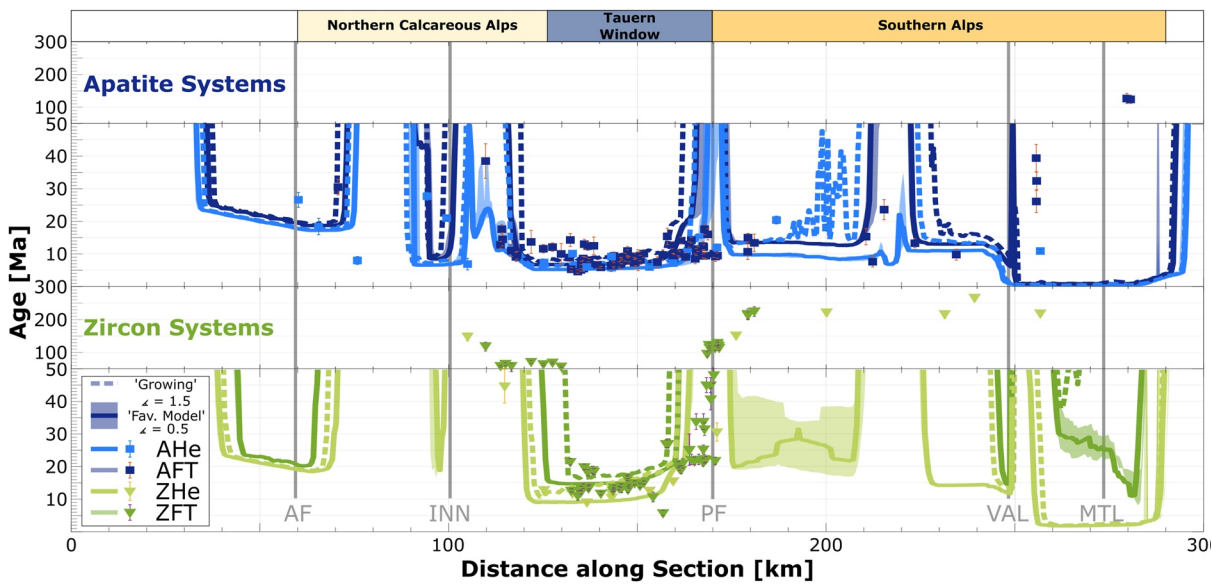

Figure 10. Thermo-kinematic model sensitivity under different topographic scenarios, that is, variable angles of tapered topography and linearly "growing" topography from model initiation (Eocene/Oligocene) to present-day level. The preferred model ("Fav. Model") adopts a tapered topography of 1° along both southern and northern orogenic wedges. AT, Alpine Frontal Thrust; INN, Inntal fault; PF, Periadriatic Fault; VAL, Valsugana/Belluno thrust system; MTL, Montello thrust system.

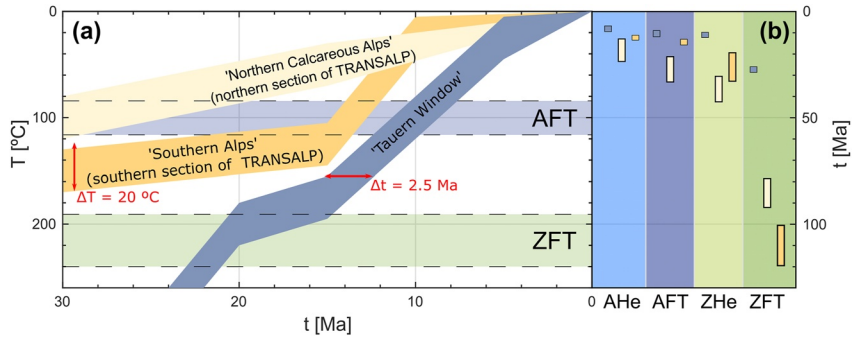

Figure 11. Range of predicted model ages for idealized, representative swaths of *t*-*T*-paths for the Northern Calcareous Alps, the Tauern Window, and the Southern Alps (see also Figure 7). (a) Idealized, representative *t*-*T*-path swaths. (b) Range of predicted thermochronometer ages for the respective scenarios. Default mineral parameters are from Ketcham et al. (2009), kinetic models from Flowers et al. (2009), Guenthner et al. (2013), Ketcham et al. (2007), and Yamada et al. (2007).

4.2.4. Effect of Topography/Erosion on Thermochronometer Ages

Different topographic boundary conditions have been applied to our preferred thermo-kinematic model. Two scenarios explore different inclinations of the tapered topography applied for each deformation step, whereas another grows topography linearly to that of present-day (Figure 10). The 2D nature of our modeling approach limits our capability to evaluate different elevations at an individual location in the same model run. Hence, age-elevation profiles cannot be produced. Each simulation represents a single topographic/erosional model, adopting a tapered topography angle range of 0.5–1.5° at each deformation step or a linear topographic growth model. Even though a tapered topography angle of 1.5°, representative of a generally steeper local gradient, produces a better statistical fit with the observed age data relative to the preferred model ($\chi^2_{score} = 40.63$; Figure 5, Table 3), it overpredicts the present-day topography (closer to 1°). An angle of 0.5° generally lowers the predicted age ranges under increased cooling through more efficient erosion, and vice versa for higher angles of 1.5°. However, topographic effects appear negligible in the model and only become apparent for the ZHe system across the Southern Alps, where age variations >20 Myr are predicted. The latter is likely related to the prolonged time spent near the ZHe system closure temperature (140°C–220°C; Guenthner et al., 2013; Figure 7) before bedrock reached the surface. Assuming a topography that linearly grows to present-day levels induces a more irregular distribution of predicted ages along the transect while increasing the overall statistical misfit relative to the preferred model ($\chi^2_{score} = 125.57$). Such a scenario, however, does not consider topographic development as a function of rock uplift due to motion along active faults and is, hence, less viable.

Table 3
Statistical Model Performances Using Reduced χ^2-Statistics

Model	Reduced χ^2 Statistic ($*10^3$)
"Favored Model"	74.00
Shortening rates by Schmid et al. (1996)	81.44
Shortening rates by Dewey et al. (1989)	70.70
Increased shortening rates ("Favored Model" + 1 mm/yr)	67.26
Reduced shortening rates ("Favored Model" − 1 mm/yr)	80.94
Low heat production ("Favored Model" at $A_0 = 1.0$ μW/m^3)	277.01
Low heat production ("Favored Model" at $A_0 = 3.0$ μW/m^3)	98.18
High heat production ("Favored Model" at $A_0 = 6.0$ μW/m^3)	54.22
"Favored Model" with "growing" topography	125.57
"Favored Model" at ∡ 1.5 tapered topography	40.63
"Favored Model" at ∡ 0.5 tapered topography	81.36

Note. Values higher than the "Favored Model" ($\chi^2_{score} = 74.00$) performed worse (>74.00), and vice versa (<74.00).

5. Discussion

5.1. Thermo-Kinematic Evolution of the Eastern Alps

Model results and cooling ages in this study suggest cooling age distributions, and *t*-*T* paths from the observed thermochronologic record are driven by exhumation in regions of active crustal deformation during the indentation of Adria into Europe since the Eocene/Oligocene. Hence, the models can be used to critically ascertain how physical processes driving collisional orogenesis and potential changes in the collisional architecture of the Eastern Alps relate to the hinterland cooling history and the times and locations of fault activity without the need to involve mantle-driven buoyancy forces.

5.1.1. Sensitivity to Thermophysical Parameters

Our model sensitivity analysis of processes influencing cooling ages investigated variations in (a) shortening rates (Figure 8), (b) crustal volumetric heat production (Figure 9), and (c) topographic evolution (Figure 10). These

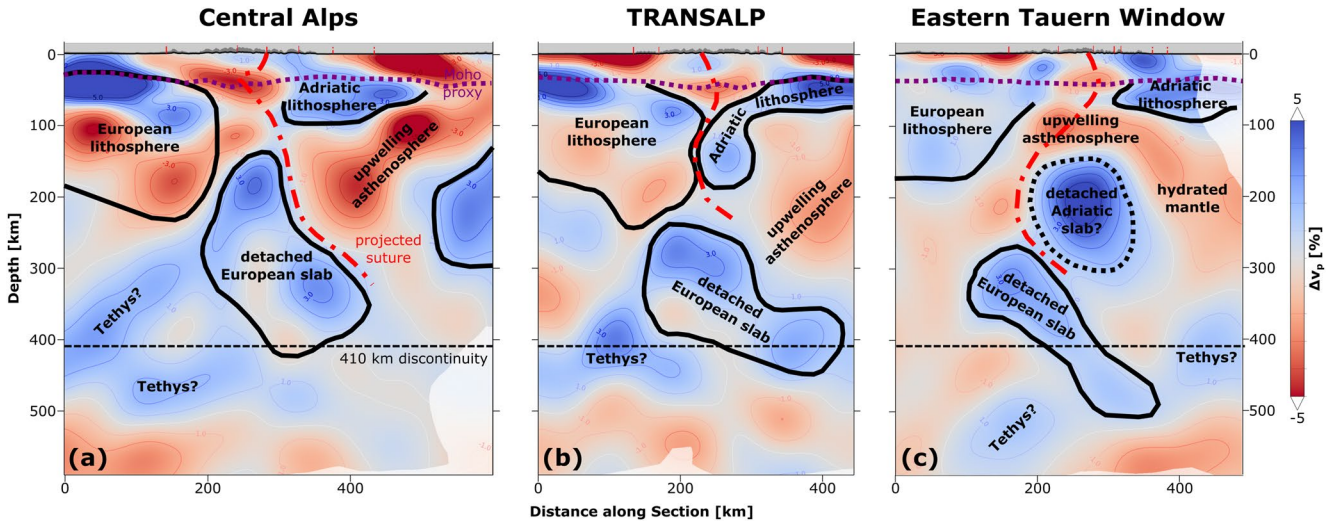

Figure 12. AlpArray *P*-wave travel time tomography slices for the wider Tauern Window region (Paffrath et al., 2021) with new proposed slab geometries, including interpretations modified from M. Handy et al. (2021). See Figure 1c for the exact location of the profiles.

factors are relevant to orogenesis of small mountain ranges such as the European Alps. In the following, we discuss how the previous factors are manifested in our sensitivity analyses.

Estimates for convergence rates between the Adriatic and European plates since the Eocene/Oligocene are around 10 mm/yr, decreasing by more than ~30% in the Early Miocene (Dewey et al., 1989; Le Breton et al., 2021; Müller et al., 2019; Ustaszewski et al., 2008). The previous convergence rate would be partitioned between upper plate shortening and subduction of the underlying plate. Applying upper plate (crustal) shortening rates of 3–4.5 mm/yr in our thermo-kinematic models and varying these by up to 2 mm/yr, including the implementation of unrealistically high crustal shortening rates of up to 9.4 mm/yr, did not yield a large reduction in the misfit between thermochronometer observations and the five different thermo-kinematic models presented (Figure 5). Nevertheless, larger variations across other convergent mountain belts such as those in the Himalaya (e.g., Ghoshal et al., 2020; Gilmore et al., 2018; McQuarrie et al., 2019) have shown that crustal shortening rates can be constrained by the low-temperature cooling record.

In addition, crustal volumetric heat production values ranging between 0.3 and 5.5 $\mu W/m^3$ across different types of sedimentary and igneous rocks (Ehlers, 2005) impose a significant effect on interpreted cooling histories. Similar heat production values have been determined along TRANSALP (Vosteen et al., 2003) and could be representative of other small mountain ranges with similar lithological heterogeneities. Predicted low-temperature thermochronometers (<120°C, AHe and AFT) in our thermo-kinematic models were sensitive to the previous range of possible crustal volumetric heat production values explored (Figure 9). Reaching lowest misfits to observed data should yield the best estimates for crustal volumetric heat production in a region applying our modeling approach. Indeed, a (high) value of 6.0 $\mu W/m^3$ yields a low misfit for the Tauern Window with respect to observed AHe and AFT ages (Figure 5, Table S1). This high value is consistent with maximum values reported from some samples in Vosteen et al. (2003).

Changes in the topography used in the simulations, such as variations in topographic taper of up to 1°, do not appear to have a significant effect on cooling age predictions along TRANSALP. The only exception to this are the predicted ZHe ages above the Dolomites (Figure 10), which might be related to its thrust-/back-thrust kinematics inducing increased erosion within the same displaced unit. Overall, we find that low-temperature thermochronometers appear poorly suited to track topographic evolution over geologic time scales within our modeling framework for the TRANSALP transect.

5.1.2. Upper Lithospheric Deformation Along TRANSALP

Under the assumption of doubly-vergent wedge mechanics, orogen-scale thermo-kinematic models may aid in identifying a subduction polarity reversal. Schlunegger and Willett (1999) applied similar principles in the

Central Alps for the pro- and retro-wedges situated above the European and the Adriatic plate (including slivers of the Iberian plate), respectively. In the Central Alps the deeply exhumed Lepontine Dome corresponds to the retro-wedge, hence subduction of Europe beneath Adria. If continental subduction polarity switched after the onset of continental collision along the TRANSALP transect, then the pro-wedge and retro-wedge locations would interchange. This process should entail a re-positioning of the locus of deepest exhumation characteristic of the retro-wedge (Willett & Brandon, 2002) if asymmetric orographic precipitation effects can be ruled out (Willett, 1999). The latter appears to be the case because wind directions have followed an east-west trajectory, that is, a North Atlantic-driven climate, since the Pliocene (e.g., Botsyun et al., 2020) or the Mid-Miocene (Methner et al., 2020). At the same time, the new pro-wedge should widen through an outwards shift of active deformation fronts with the retro-wedge slowly responding to such changes (e.g., Dal Zilio et al., 2020; Naylor & Sinclair, 2007; Naylor et al., 2005; Stockmal et al., 2007).

Our preferred structural and thermo-kinematic model (Figure 4) reflects this behavior while consistent with observed thermochronological data. Furthermore, this model does not assume any vertical motion along the PF since the Eocene/Oligocene, in line with the "crocodile model," but contrary to the "lateral extrusion model" (Castellarin et al., 2006; Lüschen et al., 2004) or reconstructions by Schmid et al. (2004). The output of this model matches to a first-order degree: (a) the orogen-scale geology along the transect; (b) the observed distribution of thermochronometer ages on the surface (Figure 6); (c) independent *t-T* path thermal inversion solutions (Figure 7); and (d) present-day heat flux values (Figure 6). Hence, this model can be used as a viable solution for the thermo-kinematic and structural evolution of the eastern European Alps along TRANSALP since the Eocene/Oligocene, despite the variabilities in thermal properties (e.g., Vosteen et al., 2003), convergence rates (Schmid et al., 1996), topographic evolution, and the presence of more complex structural geometries locally. The model performs particularly well across the Tauern Window, where thermochronologic data density is highest. More thermochronological sampling and detailed modeling work may be required across the Southern Alps and the NCA (including the Subalpine Molasse and Helvetic Units), where the thermochronologic data density is sparse despite our new fission-track data. According to our results 105 km of north-south directed crustal shortening is sufficient to reproduce the rock cooling record along TRANSALP. This suggests that a minimum of ∼50 km of convergence must have been accommodated by lateral extrusion and local, second-order fault activity not modeled in our reconstructions, when applying the more recent total shortening estimates of ∼160 km (Rosenberg et al., 2021; Ustaszewski et al., 2008). Our preferred model demonstrates that a north-to-south shift of fault activity since initial continental collision is consistent with the observed thermochronologic record. During Miocene times, deep exhumation of the Tauern Window (e.g., Bertrand et al., 2017) associated with activity along the Tauern Ramp coincides with the sequential shifting of fault activity southwards in the Southern Alps. Such a shift in fault activity appears to be coeval with a change from deep marine to shallow marine/terrestrial conditions in the eastern Molasse basin as well as the increase in subsidence rates in the Po basin (Mellere et al., 2000) that is associated with a prior slab breakoff at ∼20 Ma (M. R. Handy et al., 2015; Schlunegger & Kissling, 2022). If Adria moved beneath Europe to fill the resulting lithospheric gap, then the observed pattern of fault activity appears consistent with the expected, corresponding upper lithospheric response if doubly-vergent Coulomb wedge mechanics are applicable. Following this line of thought, present-day fault activity across the southernmost section of TRANSALP indicated by recent earthquake activity and geodetic measurements, including InSAR analyses (e.g., Anderlini et al., 2020; Moratto et al., 2019; Nocquet & Calais, 2004; Serpelloni et al., 2016), may indicate a presently ongoing southward migration of the active southern Alpine deformation front, hence a continuation of sequential deformation that initiated with activity along the Valsugana thrust system coeval with Tauern Ramp activity.

5.1.3. Tauern Window Exhumation

Miocene exhumation of the Tauern Window has long been recognized and described in detail (e.g., Bertrand et al., 2017; Lammerer et al., 2008; Rosenberg et al., 2018). Hence, correctly reproducing its thermal evolution is a minimum requirement for validating our thermo-kinematic model. Our results match the subsurface geometry suggested by the TRANSALP Working Group (Lüschen et al., 2004) and first-order, present-day surface, and subsurface structural observations (Lammerer et al., 2008; Figures 4 and 6). This concerns the attitude, location, and kinematics of major faults (the Inntal Fault, Tauern Ramp and Dolomite Ramp) assuming no vertical offset along the PF. However, second-order variations in fault geometries (Figure 1b vs. Figure 4) remain due to structural simplifications made to facilitate the modeling process. For example, shortening has been accommodated only along major faults avoiding, for example, splay faults and sub-parallel secondary faults while faults have been straightened.

The *t-T* paths extracted from our preferred model (Figure 7) describe high cooling rates since the Mid-Miocene, with surface rocks located in the central Tauern Window having originated from the highest temperature ranges (>200°C). A general slowing of exhumation followed this period since the Pliocene. The 2D model results presented in this study are consistent with recent 1D thermal history inversions of thermochronometer data from the region (Eizenhöfer et al., 2021). It should be noted, however, that our prediction of low-thermochronometer ages only captures cooling since the simulated start of shortening in the Oligocene/Miocene, not the collisional history prior to this. For records of earlier cooling relevant to the Tauern Window we refer to earlier studies (e.g., Fügenschuh et al., 1997; Glodny et al., 2005; Kurz et al., 2008; Schneider et al., 2015). Predicted low-temperature thermochronometer ages between the Inntal fault and the PF produce low statistical misfits with observed distributions suggesting that the forward modeled cooling history is viable and, hence, may be representative for the cooling history in this region. Based on the underlying structural model proposed in this study (Figure 4), this suggests a structural linkage between the Inntal fault and the Tauern Ramp and differential exhumation between the Tauern Window and the PF due to the vertical component of motion along the ramp. There, more erosion may have occurred northwards across the youngest horse of the Tauern duplex. Because of the modeled duplex kinematics, the highest temperature thermochronometer systems (ZFT; to some degree ZHe) may have preserved records of the early Miocene Tauern doming/duplexing in the region between the Tauern Window and the Inntal Fault before activity along the Tauern Ramp (Figure S1 in Supporting Information S1, deformation steps prior to 12.7 Ma). Lower temperature thermochronometer systems, on the other hand, record the phase of rapid exhumation during the activity of the Tauern Ramp. As observed across the Tauern Window, high crustal heat production values further improve the statistical fit to the observed data relative to the preferred model (AHe, $\chi^2_{score} = 0.20$; AFT, $\chi^2_{score} = 17.69$; ZHe, $\chi^2_{score} = 0.32$; ZFT, $\chi^2_{score} = 15.91$, for $A_0 = 6.0$ μW/m^3; Figure 9; Table 3 and Table S3). This is also the case assuming a higher topographic taper angle (AHe, $\chi^2_{score} = 0.29$; AFT, $\chi^2_{score} = 7.49$; ZHe, $\chi^2_{score} = 0.15$; ZFT, $\chi^2_{score} = 17.11$).

In summary, the model presented here confirms ~10 km of exhumation across the Tauern Window due to rock displacement along the Tauern Ramp, accompanied by focused erosion. Hence, the thermochronologic record is driven mainly by tectonic processes. Topographic variability (and tectonic denudation; Favaro et al., 2017) represents a secondary, negligible influence on the thermochronologic record (Figure 10). Increasing the topographic taper angle or increasing temperatures in the model improved the statistical fit (Table 3 and Table S3) across the Tauern Window suggesting that volumetric heat production was higher and/or a higher topography is more suitable. Higher elevations across the Alps have been recently proposed in the Miocene (Krsnik et al., 2021).

5.1.4. Northern Calcareous Alps Relative to the Southern Alps

Contrasting the thermal evolution across the NCA and the Southern Alps aids in evaluating their role within the doubly-vergent orogenic system. However, due to unsuitable lithology, thermochronologic data are sparse in the Northern Calcareous and Southern Alps. Suites of reset AFT ages in the Southern Alps imply surface rocks experienced higher temperatures during continental collision. This has been confirmed by 1D thermal inversions (Eizenhöfer et al., 2021; Zattin et al., 2006). Results from the thermo-kinematic models presented here suggest this difference is caused by exhumation following activity on the Valsugana/Belluno thrust system. Local age variations were likely caused by a locally more complex kinematic history (e.g., Schönborn, 1999) that has not been implemented in our structural-kinematic model. The *t-T* path solutions from our thermo-kinematic model indicate that the highest temperatures did not exceed ~200°C in the Early Miocene, followed by a steady decrease in temperatures from the Mid-Miocene onwards.

The thermo-kinematic model presented here assumes Early Miocene shortening in the NCA (including the Subalpine Molasse and Helvetic Units) along the Alpine Frontal Thrust followed by tectonic inactivity to the present day. Auer and Eisbacher (2003) suggested that considerable mid-Eocene to Oligocene shortening has taken place in the NCA, evidenced by Eocene/Oligocene sedimentary strata cut by north-directed faults. In contrast to the simplified kinematics adopted in our preferred model, shortening has likely been distributed across multiple thrust faults that feed into a common décollement beneath the NCA (e.g., Auer & Eisbacher, 2003; Ortner et al., 2015). This result explains the variation in observed ages not captured in our model (Figures 2 and 3a). Forward modeled *t-T* paths indicate that the NCA (including the Subalpine Molasse and Helvetic Units) south of the Inntal fault experienced a brief period of fast cooling in the Mid- to Late Miocene, probably associated with the Inntal fault (zone) being led into the Tauern Ramp (Ortner et al., 2006, 2015), and hence the Mid-Miocene exhumation of the Tauern Window.

These kinematic contrasts between the NCA and the Southern Alps underline the interpretation that since the Mid-Miocene, the Southern Alps not only have witnessed exhumation from higher temperatures (~50–100 K higher than in the NCA) but also have accommodated more shortening through the sequential southward shift of active deformation since then (Castellarin & Cantelli, 2000; Castellarin et al., 2006; Ustaszewski et al., 2008). Such behavior appears more akin to accretionary growth along a pro-wedge (e.g., Naylor & Sinclair, 2007). However, this behavior might also be related to the higher rigidity of the Adriatic indenter, as proposed for the Central Alps (Schmid et al., 1996). Fry et al. (2010), on the other hand, suggested that any such indenter corresponds to lower crustal material of the European Plate, and not one of Adriatic origin. Kissling and Schlunegger (2018) promote the absence of an indenter in the Central Alps. Rheological differences within the lithosphere and across the plate interface play an important role in the application of doubly-vergent Coulomb wedge mechanics. More specifically, retro-wedge deformation only takes place at sufficiently high degrees of plate interface coupling promoted by the presence of decoupling horizons in the overriding plate (Vogt et al., 2017; Willingshofer et al., 2013). Hence, the application of doubly-vergent wedge mechanics and subsequent derivation of subduction polarity from upper crustal cooling patterns requires the absence of high rheological contrasts across the European and Adriatic plates. The presence of significant deformation across both wedges along TRANSALP suggests a sufficiently high degree of inter-plate coupling. The observation that fault activity sequentially propagated southwards in the past may also explain the present-day higher seismicity in the Southern Alps (Moratto et al., 2019; Serpelloni et al., 2016) in comparison to the rather inactive northern Alps (Figure 1), indicating a continued southward shift of active deformation.

Finally, the 2D thermo-kinematic forward modeling approach used in this study considers horizontal tectonic advection in contrast to recent 1D thermal inversion models conducted in the European Alps that focused on changes in erosion rates in recent geologic time (e.g., Herman et al., 2013; Schildgen et al., 2018; Willett et al., 2020). Consideration of lateral motion is important when trying to understand how variations in structural geometry correspond to observed cooling ages. For example, prolonged time spent at a specific temperature range may imply overall tectonic quiescence at low exhumation rates. Still, it may alternatively reflect the response to horizontal displacement along low-angle fault planes during tectonic activity, such as in the Southern Alps before active rock uplift during episodes of thrusting (Figures 7 and 11). This difference cannot be distinguished in *t-T* path solutions (Figure 11). Depending on the temperature and depth in question, this may affect some observed thermochronometer systems (Figure 11). Extensive earlier nappe tectonics prevalent across the European Alps may result in apparently inconsistent cooling histories if only vertical rock motion is considered. This may be the case, for example, when a tectonic nappe is emplaced above another one with a different cooling history.

5.2. Evidence for a Mid-Miocene Subduction Polarity Reversal?

Displacement and focused exhumation across the Tauern Window occurred since at least the Oligocene/Eocene (e.g., Bertrand et al., 2017; Favaro et al., 2015, 2017; Frisch et al., 1998; Rosenberg et al., 2018; Schneider et al., 2015). Rapid exhumation associated with activity on the Tauern Ramp during the Mid-Miocene, however, appears to mark a fundamental change in orogen-wide exhumation across the Eastern Alps. This period coincides with the proposed timing of European slab detachment at 10–25 Ma (e.g., M. Handy et al., 2021; Horváth et al., 2006; Scharf et al., 2013) as well as the cessation of active deformation along the Alpine Frontal Thrust and onset of deformation in the Southern Alps at 20 Ma (e.g., Ustaszewski et al., 2008). Before the onset of continental collision, a southward subduction geometry was potentially driven by high European slab loads (e.g., Schlunegger & Kissling, 2022). During the Early Miocene, exhumation across the Tauern Window continued, contemporaneous with shortening across the NCA and on the Alpine Frontal Thrust. Higher temperature thermochronometers, such as ZFT and muscovite $^{40}Ar/^{39}Ar$, may have preserved a record of this early Tauern exhumation not associated with the Tauern Ramp (Figure 6; Figure S1 in Supporting Information S1; see Schneider et al., 2015). Such upper crustal fault responses and exhumation patterns are in accordance with the initial pro- and retro-wedge positions north and south of the PF as proposed by most recent studies (e.g., M. Handy et al., 2021). However, the situation in the Southern Alps until the Mid-Miocene requires further investigation to resolve its retro-wedge position during this time. Higher temperatures (Figure 7) and deeper-rooted exhumation in the Southern Alps (in relation to the NCA) may have recorded this Oligocene/Eocene to Early Miocene retro-wedge position of the Southern Alps.

Modeling results presented here suggest that Mid-Miocene activity of the Tauern Ramp, the NCA (including the Subalpine Molasse and Helvetic Units) is consistent with previous work (e.g., Ustaszewski et al., 2008). Coevally,

the Southern Alps initiated a southward shift in fault activity and exhumation, that is, shifting in sequence from the Valsugana/Belluno to the Montello thrust system. This southward propagation appears to be presently ongoing along the southernmost section of the TRANSALP transect, indicated by high seismic potentials (e.g., Anderlini et al., 2020; Moratto et al., 2019; Nocquet & Calais, 2004; Serpelloni et al., 2016). If Mid-Miocene Tauern Ramp activity, characterized by fast and deep-seated exhumation is interpreted as an orogen-scale mega retro-thrust then the region north of the PF would be more akin to a present-day retro-wedge. Consequently, the sequential temporal shift of active deformation southwards across the Southern Alps would indicate the accommodation of increased accretionary flux from the south. This interpretation would be more consistent with deformation along a pro-wedge. Following this line of thinking, then these upper lithospheric responses observed in the bedrock cooling record and supported by our preferred thermo-kinematic model are best reconciled by a response to a fundamental change in the doubly-vergent orogenic wedge mechanical framework since the Mid-Miocene subsequent to Adriatic indentation after European slab break-off at ∼20 Ma. This conclusion necessitates that doubly-vergent Coulomb wedge theory can be applied along the TRANSALP transect, such that: (a) the required horizontal forces are present, and (b) the European and Adriatic plates are sufficiently coupled across the plate interface in the potential presence of decoupling horizons in the overriding plate (Vogt et al., 2017; Willingshofer et al., 2013). The latter requirement (b) can be assumed due to the presence of coeval crustal deformation across both orogenic wedges. Alternative tectonic processes or plate configurations predicting the same across-strike, orogen-scale reorganization of fault activity and exhumation (in the absence of a subduction polarity reversal) have not yet been presented by previous work.

Despite recent seismic interpretations (M. Handy et al., 2021; Paffrath et al., 2021; Figure 12) that suggest a continuous, vertical to overturned European slab before its detachment at ∼25–10 Ma, the possibility remains open for a (potentially ongoing) reversal from the Mid-Miocene onwards (Eizenhöfer et al., 2021) facilitated by a wedge of Adriatic plate material into space provided by a European slab break-off event at ∼20 Ma (M. R. Handy et al., 2015; Schlunegger & Kissling, 2022). This interpretation is contrary to the interpretation by M. Handy et al. (2021). Instead, high-velocity anomalies at ∼150 km depth beneath the present-day Southern Alps may be associated with Adriatic lithosphere that penetrated the gap caused by European slab break-off (Figure 12). According to this interpretation, a minimum of ∼100 km of Adriatic lithosphere would have been subducted since the hypothetical Mid-Miocene reversal of continental subduction. This would require 109–113 km of shortening north of the PF across the Tauern Window in addition to >50 km in the Southern Alps (Ustaszewski et al., 2008; and references therein). This line of thought is fully compatible with average plate tectonic convergence rates of ∼7 mm/yr since the Mid-Miocene (Le Breton et al., 2021). Figure 12 only shows the most recent mantle tomographic image (i.e., Paffrath et al., 2021). Alternative images for the region have been published in the past (e.g., Behm et al., 2007; Brückl et al., 2010; Hetényi et al., 2018; Kästle et al., 2020; Kind et al., 2021; Lippitsch, 2002; Lippitsch et al., 2003; Mitterbauer et al., 2011; Plomerová et al., 2022). However, a full review of existing tomographic images is beyond the scope of this study, and we refer instead to Kästle et al. (2020) or M. Handy et al. (2021). Hence, a subduction of the European lithosphere before European slab detachment at ∼25–10 Ma (M. Handy et al., 2021) followed by a Mid-Miocene (potentially ongoing) reversal of continental subduction (Eizenhöfer et al., 2021), resulting in a wedge of Adriatic lithosphere into European, could have been facilitated by a European slab break-off at 20 Ma. This interpretation is consistent with observations such as: (a) the general southward shift of crustal fault activity along TRANSALP suggested by our thermo-kinematic modeling; (b) recent plate tectonic reconstructions across the Mediterranean (Le Breton et al., 2021; Müller et al., 2019); (c) stratigraphic evidence from the Molasse and Po basins (Schlunegger & Kissling, 2022); and (d) most-recent seismic AlpArray tomography (Paffrath et al., 2021; Figure 12).

5.3. Study Limitations

Given the heterogeneity of the European Alps along the TRANSALP geophysical transect with respect to lithology, thermophysical characteristics, and structural geometry, our model setup was simplified to enhance an understanding of the region (orogen) scale thermal processes. The model limitations discussed below provide a framework for more detailed future thermo-kinematic and structural modeling work conducted over smaller spatial scales. In our thermo-kinematic models, several assumptions were made that resulted from either technical restrictions placed by the thermo-kinematic model used, or a necessary reduction in model complexity to find a meaningful balance between modeling time and the additional insights gained.

First, lateral extrusion tectonics have long been described in the Eastern Alps (Frisch et al., 1998; Linzer et al., 2002; Ratschbacher, Frisch, et al., 1991; Ratschbacher, Merle, et al., 1991) and are manifested by strike-slip activity along the Inntal fault and PF during the Oligocene and Neogene, respectively (e.g., Bartosch et al., 2017; and references therein). Extrusion tectonics have not been implemented into our modeling approach. However, we do not expect lateral motion of material from extrusion tectonics to meaningfully affect our interpretation of the reconstructed cooling history because: (a) the rotation of Adria into the Eastern Alps since ∼35 Ma caused north-south oriented shortening along TRANSALP (e.g., Le Breton et al., 2021; Rosenberg et al., 2018) which is captured within our reconstructions; (b) although lateral extrusion accommodates plate tectonic shortening, compressional structures are still required to induce rock exhumation and erosional cooling such as that associated with Tauern Ramp activity. The exception to this being normal faults such as the Brenner and Katschberg faults to the west and east of TRANSALP, respectively (e.g., Lammerer & Weger, 1998; Wolff et al., 2021), which exhibit significant breaks in metamorphic isotherms; (c) lateral motion is primarily subparallel to subsurface isotherms due to extrusion tectonics and is not expected to contribute significantly to erosional cooling; and (d) the faults responsible for active rock uplift in our models (the Alpine Frontal Thrust, the Inntal fault and SEMP) continue laterally over sufficiently large distances that exceed the maximum amount of lateral extrusion (∼170 km, Frisch et al., 1998; >120 km, Linzer et al., 2002). Given that our predicted north-south shortening of ∼105 km is smaller than the total amount (∼160 km) of convergence in the Eastern Alps estimated by recent studies (Rosenberg et al., 2015; Ustaszewski et al., 2008), a minimum of ∼55 km of convergence must have been accommodated by structures other than the main thrust faults incorporated in our model. This value is close to an estimate of ∼40 km ductile north-south shortening in the Tauern Window that was accompanied by orogen-parallel stretching but negligible crustal thickening (Lammerer & Weger, 1998). As a result, our model provides low estimates of orogenic shortening in comparison to recent estimates (Rosenberg et al., 2021). Consequently, existing cross-sections cannot be regarded as "balanced" sensu strictu (Dahlstrom, 1969; Schönborn, 1999; Suppe, 1983, 1985).

Second, crustal thickening in the modeling approach presented here assumes diffuse deformation beneath the active décollement that thickens the crust and displaces the Moho to higher depths. This process eventually leads to the development of a "lower crustal bulge." This entails that displaced mass between the active décollement and the modeled Moho is preserved throughout the kinematic modeling process, however, without providing precise kinematics for its distribution after each deformation step. We acknowledge that this approach is not able to capture surface responses to mantle processes such as slab delamination. Such processes require alternative approaches, for example, geodynamic modeling. In addition, even though modeled Moho deformation precisely reflects the area increase due to crustal thickening in the model, it does not constrain the location of crustal thickening. In our approach the modeled Moho is warped toward its present-day location as identified by Kummerow et al. (2004) in each deformation step.

Third, we assumed a simplified tapered wedge topographic evolution along both Coloumb-wedges in the north and south throughout each model run. Furthermore, potential surface uplift following European slab delamination (e.g., Kissling & Schlunegger, 2018; Schlunegger & Kissling, 2022) is not considered in our model and, hence, results in a present-day 0 m elevation for the Northern Alpine Molasse Basin. This study does not accurately evaluate smaller-scale topographic variations or changes in topographic relief or mean elevation associated climatic change such as glacial erosion.

Fourth, tectonic denudation facilitated by activity along the Katschberg and Brenner normal faults east and west of the Tauern Window, respectively, contributed only to a third of its Miocene exhumation (e.g., Favaro et al., 2017). These processes have not been taken into account here. As a result, thrust-related exhumation may be locally overestimated.

6. Conclusions

This study investigated whether the low-temperature rock cooling record along the TRANSALP geophysical transect can provide new constraints to thermal and deformation processes in small convergent mountain ranges, such as in the eastern European Alps. Structural kinematics derived from generalized upper lithospheric balanced cross-sections resulted in an updated subsurface geometry beneath the transect (Figure 1b), consistent with the Neogene structural evolution of the region described in the literature. This cross-section, when inte-

grated into a thermo-kinematic model, was used to explore crustal exhumation as a function of orogen-scale fault activity.

Similar to the "crocodile model" by the TRANSALP Working Group (Lüschen et al., 2004), the kinematic model presented here does not require significant vertical motion along the PF. We presented a suite of thermo-kinematic forward models that tested sensitivities related to variable thermophysical properties, convergence rates, and topographic evolution along TRANSALP where low-temperature thermochronometers (<120°C; AHe and AFT) appear most sensitive to these factors. When compared to observations, model predictions led to a viable solution for the thermo-kinematic evolution along the transect, validated by the observed geology and thermal field as constrained by thermochronologic age distributions and *t-T* history as well as present-day heat flow. Based on the results of our modeling experiments, we identify a primarily tectonic origin for the thermal history along the transect. In contrast, variations in thermophysical properties, convergence rates, and topographic evolution are secondary.

If crustal structural responses are reflective of the lower lithospheric subduction polarity along the TRANSALP transect, then the model supports the hypothesis of a significant Mid-Miocene reorganization of continental collision processes in the Eastern Alps with the onset of rapid exhumation of the Tauern Window during Tauern Ramp activity. Interpreting the Tauern Ramp as an orogen-scale mega retro-thrust would be indicative of a retro-wedge position, and the southward propagation of fault activity in the Southern Alps characteristic of pro-wedge behavior. This line of arguments implies a reversal in continental subduction polarity since the Mid-Miocene that may have been enabled through Adriatic indentation through a lithospheric window. Following this thought, the subduction polarity reversal potentially commenced with break-off of the European slab at ~20 Ma. Alternatively, strong rheological differences across the involved plates would be required that disconnect upper lithospheric deformation from lower lithospheric processes. However, it remains unclear whether this alternative scenario can offer a plausible explanation for the observed north-south contrast in exhumation and faulting patterns in the Eastern Alps.

Data Availability Statement

Our new structural-kinematic model and thermochronology data, including thermo-kinematic model input and output, can be accessed from the GFZ Data Services (Eizenhöfer et al., 2023; https://doi.org/10.5880/fidgeo.2022.017). The University of Tübingen specific version "Pecube-D" is available on Zenodo (Ehlers, 2023; https://doi.org/10.5281/zenodo.7785668). Seismic data were taken from the International Seismological Center (Storchak et al., 2017) and the GEOFON Data Center (1993). Digital elevation models were produced by the U.S./Japan ASTER Science Team (2000). Receiver function analysis was adopted from Kummerow et al. (2004). AlpArray tomography slices are from M. Handy et al. (2021) and Paffrath et al. (2021).

Acknowledgments
We would like to thank the Editor and reviews by Fritz Schlunegger and three anonymous reviewers for comments on the manuscript. This manuscript benefitted from discussions with Eline Le Breton (FU Berlin) and Mark Handy (FU Berlin). Willi Kappler (University of Tübingen) provided invaluable technical assistance. We express our gratitude to Petroleum Experts for providing academic access to MOVE™ software. This study was financed by the German Science Foundation DFG within the priority program 4D-MB and contributes to the AlpArray initiative through the following DFG Grants: GL724/8-1 to C.G., KL495/28-1 to J.K., EH329/25-1 and EH329/26-1 to T.A.E and EI1176/1-1 to P.R.E. Open Access funding enabled and organized by Projekt DEAL.

References

Agard, P., & Handy, M. R. (2021). Ocean subduction dynamics in the Alps. *Elements: An International Magazine of Mineralogy, Geochemistry, and Petrology*, *17*(1), 9–16. https://doi.org/10.2138/gselements.17.1.9

Anderlini, L., Serpelloni, E., Tolomei, C., De Martini, P. M., Pezzo, G., Gualandi, A., & Spada, G. (2020). New insights into active tectonics and seismogenic potential of the Italian Southern Alps from vertical geodetic velocities. *Solid Earth*, *11*(5), 1681–1698. https://doi.org/10.5194/se-11-1681-2020

Andeweg, B., & Cloetingh, S. A. P. L. (1998). Flexure and 'unflexure' of the North Alpine German-Austrian Molasse Basin: Constraints from forward tectonic modelling. *Geological Society, London, Special Publications*, *134*(1), 403–422. https://doi.org/10.1144/gsl.sp.1998.134.01.19

Anselmi, M., Govoni, A., De Gori, P., & Chiarabba, C. (2011). Seismicity and velocity structures along the south-Alpine thrust front of the Venetian Alps (NE-Italy). *Tectonophysics*, *513*(1–4), 37–48. https://doi.org/10.1016/j.tecto.2011.09.023

Argand, E. (1916). Sur l'arc des Alpes occidentales. *Ecologae Geologicae Helvetiae*, *14*, 145–191.

Auer, M., & Eisbacher, G. H. (2003). Deep structure and kinematics of the Northern Calcareous Alps (TRANSALP profile). *International Journal of Earth Sciences*, *92*(2), 210–227. https://doi.org/10.1007/s00531-003-0316-0

Babuška, V., Plomerova, J., & Granet, M. (1990). The deep lithosphere in the Alps: A model inferred from P residuals. *Tectonophysics*, *176*(1–2), 137–165. https://doi.org/10.1016/0040-1951(90)90263-8

Barnhart, K. R., Tucker, G. E., Doty, S. G., Shobe, C. M., Glade, R. C., Rossi, M. W., & Hill, M. C. (2020a). Inverting topography for landscape evolution model process representation: 1. Conceptualization and sensitivity analysis. *Journal of Geophysical Research: Earth Surface*, *125*(7), e2018JF004961. https://doi.org/10.1029/2018jf004961

Barnhart, K. R., Tucker, G. E., Doty, S. G., Shobe, C. M., Glade, R. C., Rossi, M. W., & Hill, M. C. (2020b). Inverting topography for landscape evolution model process representation: 2. Calibration and validation. *Journal of Geophysical Research: Earth Surface*, *125*(7), e2018JF004963. https://doi.org/10.1029/2018JF004963

Bartosch, T., Stüwe, K., & Robl, J. (2017). Topographic evolution of the Eastern Alps: The influence of strike-slip faulting activity. *Lithosphere*, *9*(3), 384–398. https://doi.org/10.1130/l594.1

Beaumont, C., Kamp, P. J., Hamilton, J., & Fullsack, P. (1996). The continental collision zone, South Island, New Zealand: Comparison of geodynamical models and observations. *Journal of Geophysical Research*, *101*(B2), 3333–3359. https://doi.org/10.1029/95jb02401

Behm, M., Brückl, E., Chwatal, W., & Thybo, H. (2007). Application of stacking and inversion techniques to three-dimensional wide-angle reflection and refraction seismic data of the Eastern Alps. *Geophysical Journal International*, *170*(1), 275–298. https://doi.org/10.1111/j.1365-246x.2007.03393.x

Bertrand, A., Rosenberg, C., Rabaute, A., Herman, F., & Fügenschuh, B. (2017). Exhumation mechanisms of the Tauern Window (Eastern Alps) inferred from apatite and zircon fission track thermochronology. *Tectonics*, *36*(2), 207–228. https://doi.org/10.1002/2016tc004133

Boston, K. R., Rubatto, D., Hermann, J., Engi, M., & Amelin, Y. (2017). Geochronology of accessory allanite and monazite in the Barrovian metamorphic sequence of the Central Alps, Switzerland. *Lithos*, *286*, 502–518. https://doi.org/10.1016/j.lithos.2017.06.025

Botsyun, S., Ehlers, T. A., Mutz, S. G., Methner, K., Krsnik, E., & Mulch, A. (2020). Opportunities and challenges for paleoaltimetry in "small" orogens: Insights from the European Alps. *Geophysical Research Letters*, *47*(4), e2019GL086046. https://doi.org/10.1029/2019gl086046

Brandon, M. T., Roden-Tice, M. K., & Garver, J. I. (1998). Late Cenozoic exhumation of the Cascadia accretionary wedge in the Olympic Mountains, northwest Washington State. *Geological Society of America Bulletin*, *110*(8), 985–1009. https://doi.org/10.1130/0016-7606(1998)110<0985:lceotc>2.3.co;2

Braun, J. (2003). Pecube: A new finite-element code to solve the 3D heat transport equation including the effects of a time-varying, finite amplitude surface topography. *Computers & Geosciences*, *29*(6), 787–794. https://doi.org/10.1016/s0098-3004(03)00052-9

Brückl, E., Behm, M., Decker, K., Grad, M., Guterch, A., Keller, G. R., & Thybo, H. (2010). Crustal structure and active tectonics in the Eastern Alps. *Tectonics*, *29*(2), TC2011. https://doi.org/10.1029/2009tc002491

Caputo, R., Poli, M. E., & Zanferrari, A. (2010). Neogene–Quaternary tectonic stratigraphy of the eastern Southern Alps, NE Italy. *Journal of Structural Geology*, *32*(7), 1009–1027. https://doi.org/10.1016/j.jsg.2010.06.004

Castellarin, A., & Cantelli, L. (2000). Neo-Alpine evolution of the southern Eastern Alps. *Journal of Geodynamics*, *30*(1–2), 251–274. https://doi.org/10.1016/s0264-3707(99)00036-8

Castellarin, A., Nicolich, R., Fantoni, R., Cantelli, L., Sella, M., & Selli, L. (2006). Structure of the lithosphere beneath the Eastern Alps (southern sector of the TRANSALP transect). *Tectonophysics*, *414*(1–4), 259–282. https://doi.org/10.1016/j.tecto.2005.10.013

Channell, J. E. T. (1992). Paleomagnetic data from Umbria (Italy) : Implications for the rotation of Adria and Mesozoic apparent polar wander paths. *Tectonophysics*, *216*(3–4), 365–378. https://doi.org/10.1016/0040-1951(92)90406-v

Coyle, D. A. (1992). *The application of apatite fission track analysis to problems in tectonics*. La Trobe University.

Crowley, K. D. (1991). Thermal history of Michigan Basin and Southern Canadian Shield from apatite fission track analysis. *Journal of Geophysical Research*, *96*(B1), 697–711. https://doi.org/10.1029/90jb02174

Dahlen, F. A., Suppe, J., & Davis, D. (1984). Mechanics of fold-and-thrust belts and accretionary wedges: Cohesive Coulomb theory. *Journal of Geophysical Research*, *89*(B12), 10087–10101. https://doi.org/10.1029/jb089ib12p10087

Dahlstrom, C. D. A. (1969). Balanced cross sections. *Canadian Journal of Earth Sciences*, *6*(4), 743–757. https://doi.org/10.1139/e69-069

Dal Zilio, L., Ruh, J., & Avouac, J.-P. (2020). Structural evolution of orogenic wedges: Interplay between erosion and weak décollements. *Tectonics*, *39*(10), e2020TC006210. https://doi.org/10.1029/2020tc006210

Dando, B. D. E., Stuart, G. W., Houseman, G. A., Hegedüs, E., Brückl, E., & Radovanović, S. (2011). Teleseismic tomography of the mantle in the Carpathian-Pannonian region of central Europe. *Geophysical Journal International*, *186*(1), 11–31. https://doi.org/10.1111/j.1365-246x.2011.04998.x

Davis, D., Suppe, J., & Dahlen, F. A. (1983). Mechanics of fold-and-thrust belts and accretionary wedges. *Journal of Geophysical Research*, *88*(B2), 1153–1172. https://doi.org/10.1029/jb088ib02p01153

Dewey, J. F., Helman, M. L., Knott, S. D., Turco, E., & Hutton, D. H. W. (1989). Kinematics of the western Mediterranean. *Geological Society, London, Special Publications*, *45*(1), 265–283. https://doi.org/10.1144/gsl.sp.1989.045.01.15

Donelick, R. A., O'Sullivan, P. B., & Ketcham, R. A. (2005). Apatite fission-track analysis. *Reviews in Mineralogy and Geochemistry*, *58*(1), 49–94. https://doi.org/10.2138/rmg.2005.58.3

Ehlers, T. A. (2005). Crustal thermal processes and the interpretation of thermochronometer data. *Reviews in Mineralogy and Geochemistry*, *58*(1), 315–350. https://doi.org/10.2138/rmg.2005.58.12

Ehlers, T. A. (2023). Pecube-D: Thermokinematic and Erosion modeling software for problems in tectonics and surface processes (1.0 (stable)). *Zenodo*. https://doi.org/10.5281/zenodo.7785668

Eizenhöfer, P. R., Glotzbach, C., Büttner, L., Kley, J., & Ehlers, T. A. (2021). Turning the orogenic switch: Slab-reversal in the Eastern Alps recorded by low-temperature thermochronology. *Geophysical Research Letters*, *48*(6), e2020GL092121. https://doi.org/10.1029/2020gl092121

Eizenhöfer, P. R., Glotzbach, C., Kley, J., & Ehlers, T. A. (2023). *TRANSALP—Fission track data and thermo-kinematic model*. GFZ Data Services. https://doi.org/10.5880/fidgeo.2022.017

Farley, K. A. (2000). Helium diffusion from apatite: General behavior as illustrated by Durango fluorapatite. *Journal of Geophysical Research*, *105*(B2), 2903–2914. https://doi.org/10.1029/1999jb900348

Favaro, S., Handy, M. R., Scharf, A., & Schuster, R. (2017). Changing patterns of exhumation and denudation in front of an advancing crustal indenter, Tauern Window (Eastern Alps). *Tectonics*, *36*(6), 1053–1071. https://doi.org/10.1002/2016tc004448

Favaro, S., Schuster, R., Handy, M. R., Scharf, A., & Pestal, G. (2015). Transition from orogen-perpendicular to orogen-parallel exhumation and cooling during crustal indentation—Key constraints from $^{147}Sm/^{144}Nd$ and $^{87}Rb/^{87}Sr$ geochronology (Tauern Window, Alps). *Tectonophysics*, *665*, 1–16. https://doi.org/10.1016/j.tecto.2015.08.037

Flowers, R. M., Ketcham, R. A., Shuster, D. L., & Farley, K. A. (2009). Apatite (U–Th)/He thermochronometry using a radiation damage accumulation and annealing model. *Geochimica et Cosmochimica Acta*, *73*(8), 2347–2365. https://doi.org/10.1016/j.gca.2009.01.015

Forte, A. M., Cowgill, E., & Whipple, K. X. (2014). Transition from a singly vergent to doubly vergent wedge in a young orogen: The Greater Caucasus. *Tectonics*, *33*(11), 2077–2101. https://doi.org/10.1002/2014tc003651

Fox, M., Herman, F., Willett, S. D., & Schmid, S. M. (2016). The exhumation history of the European Alps inferred from linear inversion of thermochronometric data. *American Journal of Science*, *316*(6), 505–541. https://doi.org/10.2475/06.2016.01

Frisch, W., Kuhlemann, J., Dunkl, I., & Brügel, A. (1998). Palinspastic reconstruction and topographic evolution of the Eastern Alps during late Tertiary tectonic extrusion. *Tectonophysics*, *297*(1–4), 1–15. https://doi.org/10.1016/s0040-1951(98)00160-7

Fry, B., Deschamps, F., Kissling, E., Stehly, L., & Giardini, D. (2010). Layered azimuthal anisotropy of Rayleigh wave phase velocities in the European Alpine lithosphere inferred from ambient noise. *Earth and Planetary Science Letters*, *297*(1–2), 95–102. https://doi.org/10.1016/j.epsl.2010.06.008

Fügenschuh, B., Seward, D., & Mancktelow, N. (1997). Exhumation in a convergent orogen: The western Tauern window. *Terra Nova*, *9*(5-6), 213–217. https://doi.org/10.1046/j.1365-3121.1997.d01-33.x

Garver, J. I. (2003). Etching zircon age standards for fission-track analysis. *Radiation Measurements*, *37*(1), 47–53. https://doi.org/10.1016/s1350-4487(02)00127-0

Garzanti, E., & Malusà, M. G. (2008). The Oligocene Alps: Domal unroofing and drainage development during early orogenic growth. *Earth and Planetary Science Letters*, *268*(3–4), 487–500. https://doi.org/10.1016/j.epsl.2008.01.039

Gebrande, H., Lüschen, E., Bopp, M., Bleibinhaus, F., Lammerer, B., Oncken, O., et al. (2002). First deep seismic reflection images of the Eastern Alps reveal giant crustal wedges and transcrustal ramps. *Geophysical Research Letters*, *29*(10), 92-1. https://doi.org/10.1029/2002gl014911

Genser, J., Cloetingh, S. A. P. L., & Neubauer, F. (2007). Late orogenic rebound and oblique Alpine convergence: New constraints from subsidence analysis of the Austrian Molasse basin. *Global and Planetary Change*, *58*(1–4), 214–223. https://doi.org/10.1016/j.gloplacha.2007.03.010

GEOFON Data Centre. (1993). *GEOFON seismic network*. Deutsches GeoForschungsZentrum GFZ. Other/Seismic Network.

Ghoshal, S., McQuarrie, N., Robinson, D. M., Adhikari, D. P., Morgan, L. E., & Ehlers, T. A. (2020). Constraining central Himalayan (Nepal) fault geometry through integrated thermochronology and thermokinematic modeling. *Tectonics*, *39*(9), e2020TC006399. https://doi.org/10.1029/2020tc006399

Gilmore, M. E., McQuarrie, N., Eizenhöfer, P. R., & Ehlers, T. A. (2018). Testing the effects of topography, geometry, and kinematics on modeled thermochronometer cooling ages in the eastern Bhutan Himalaya. *Solid Earth*, *9*(3), 599–627. https://doi.org/10.5194/se-9-599-2018

Gleadow, A. J. W. (1981). Fission-track dating methods: What are the real alternatives? *Nuclear Tracks*, *5*(1–2), 3–14. https://doi.org/10.1016/0191-278x(81)90021-4

Glodny, J., Ring, U., Kühn, A., Gleissner, P., & Franz, G. (2005). Crystallization and very rapid exhumation of the youngest Alpine eclogites (Tauern Window, Eastern Alps) from Rb/Sr mineral assemblage analysis. *Contributions to Mineralogy and Petrology*, *149*(6), 699–712. https://doi.org/10.1007/s00410-005-0676-5

Grundmann, G., & Morteani, G. (1985). The young uplift and thermal history of the central Eastern Alps (Austria/Italy), evidence from apatite fission track ages. *Jahrbuch der Geologischen Bundesanstait*, *128*, 197–216.

Guenthner, W. R., Reiners, P. W., Ketcham, R. A., Nasdala, L., & Giester, G. (2013). Helium diffusion in natural zircon: Radiation damage, anisotropy, and the interpretation of zircon (U-Th)/He thermochronology. *American Journal of Science*, *313*(3), 145–198. https://doi.org/10.2475/03.2013.01

Gusterhuber, J., Dunkl, I., Hinsch, R., Linzer, H.-G., & Sachsenhofer, R. (2012). Neogene uplift and erosion in the Alpine Foreland Basin (Upper Austria and Salzburg). *Geologica Carpathica*, *63*(4), 295–305. https://doi.org/10.2478/v10096-012-0023-5

Handy, M., Schmid, S., Paffrath, M., & Friederich, W., & AlpArray Working Group. (2021). European tectosphere and slabs beneath the greater Alpine area–Interpretation of mantle structure in the Alps-Apennines-Pannonian region from teleseismic Vp studies. In *Solid Earth discussions* (pp. 1–61).

Handy, M. R., Ustaszewski, K., & Kissling, E. (2015). Reconstructing the Alps–Carpathians–Dinarides as a key to understanding switches in subduction polarity, slab gaps and surface motion. *International Journal of Earth Sciences*, *104*(1), 1–26. https://doi.org/10.1007/s00531-014-1060-3

Hardy, S., McClay, K., & Muñoz, J. A. (2009). Deformation and fault activity in space and time in high-resolution numerical models of doubly vergent thrust wedges. *Marine and Petroleum Geology*, *26*(2), 232–248. https://doi.org/10.1016/j.marpetgeo.2007.12.003

Heberer, B., Reverman, R. L., Fellin, M. G., Neubauer, F., Dunkl, I., Zattin, M., et al. (2017). Postcollisional cooling history of the Eastern and Southern Alps and its linkage to Adria indentation. *International Journal of Earth Sciences*, *106*(5), 1557–1580. https://doi.org/10.1007/s00531-016-1367-3

Herman, F., Seward, D., Valla, P. G., Carter, A., Kohn, B., Willett, S. D., & Ehlers, T. A. (2013). Worldwide acceleration of mountain erosion under a cooling climate. *Nature*, *504*(7480), 423–426. https://doi.org/10.1038/nature12877

Hetényi, G., Plomerová, J., Bianchi, I., Exnerová, H. K., Bokelmann, G., Handy, M. R., et al. (2018). From mountain summits to roots: Crustal structure of the Eastern Alps and Bohemian Massif along longitude 13.3E. *Tectonophysics*, *744*, 239–255. https://doi.org/10.1016/j.tecto.2018.07.001

Horváth, F., Bada, G., Szafián, P., Tari, G., Ádám, A., & Cloetingh, S. (2006). Formation and deformation of the Pannonian Basin: Constraints from observational data. *Geological Society, London, Memoirs*, *32*(1), 191–206. https://doi.org/10.1144/gsl.mem.2006.032.01.11

Hülscher, J., Fischer, G., Grunert, P., Auer, G., & Bernhardt, A. (2019). Selective recording of tectonic forcings in an Oligocene/Miocene submarine channel system: Insights from new age constraints and sediment volumes from the Austrian Northern Alpine foreland basin. *Frontiers of Earth Science*, *28*, 302. https://doi.org/10.3389/feart.2019.00302

Hülscher, J., Sobel, E. R., Verwater, V., Groß, P., Chew, D., & Bernhardt, A. (2021). Detrital apatite geochemistry and thermochronology from the Oligocene/Miocene Alpine foreland record the early exhumation of the Tauern Window. *Basin Research*, *33*(6), 3021–3044. https://doi.org/10.1111/bre.12593

Hurford, A. J., & Green, P. F. (1983). The zeta age calibration of fission-track dating. *Chemical Geology*, *41*, 285–317. https://doi.org/10.1016/s0009-2541(83)80026-6

Hurtig, E. (1995). Temperature and heat-flow density along European transcontinental profiles. *Tectonophysics*, *244*(1–3), 75–83. https://doi.org/10.1016/0040-1951(94)00218-x

Karousová, H., Plomerová, J., & Babuška, V. (2013). Upper-mantle structure beneath the southern Bohemian Massif and its surroundings imaged by high-resolution tomography. *Geophysical Journal International*, *194*(2), 1203–1215. https://doi.org/10.1093/gji/ggt159

Kästle, E. D., El-Sharkawy, A., Boschi, L., Meier, T., Rosenberg, C., Bellahsen, N., et al. (2018). Surface wave tomography of the Alps using ambient-noise and earthquake phase velocity measurements. *Journal of Geophysical Research: Solid Earth*, *123*(2), 1770–1792. https://doi.org/10.1002/2017jb014698

Kästle, E. D., Rosenberg, C., Boschi, L., Bellahsen, N., Meier, T., & El-Sharkawy, A. (2020). Slab break-offs in the Alpine subduction zone. *International Journal of Earth Sciences*, *109*(2), 1–17. https://doi.org/10.1007/s00531-020-01821-z

Ketcham, R. A., Carter, A., Donelick, R. A., Barbarand, J., & Hurford, A. J. (2007). Improved modeling of fission-track annealing in apatite. *American Mineralogist*, *92*(5–6), 799–810. https://doi.org/10.2138/am.2007.2281

Ketcham, R. A., Donelick, R. A., Balestrieri, M. L., & Zattin, M. (2009). Reproducibility of apatite fission-track length data and thermal history reconstruction. *Earth and Planetary Science Letters*, *284*(3–4), 504–515. https://doi.org/10.1016/j.epsl.2009.05.015

Kilian, S., Ortner, H., & Schneider-Muntau, B. (2021). Buckle folding in the Northern Calcareous Alps-Field observations and numeric experiments. *Journal of Structural Geology*, *150*, 104416. https://doi.org/10.1016/j.jsg.2021.104416

Kind, R., Schmid, S. M., Yuan, X., Heit, B., & Meier, T. (2021). Moho and uppermost mantle structure in the Alpine area from S-to-P converted waves. *Solid Earth*, *12*(11), 2503–2521. https://doi.org/10.5194/se-12-2503-2021

Kissling, E., & Schlunegger, F. (2018). Rollback orogeny model for the evolution of the Swiss Alps. *Tectonics*, *37*(4), 1097–1115. https://doi.org/10.1002/2017tc004762

Kissling, E., Schmid, S. M., Lippitsch, R., Ansorge, J., & Fügenschuh, B. (2006). Lithosphere structure and tectonic evolution of the Alpine arc: New evidence from high-resolution teleseismic tomography. *Geological Society, London, Memoirs*, *32*(1), 129–145. https://doi.org/10.1144/gsl.mem.2006.032.01.08

Klotz, T., Pomella, H., Reiser, M., Fügenschuh, B., & Zattin, M. (2019). Differential uplift on the boundary between the Eastern and the Southern European Alps: Thermochronologic constraints from the Brenner Base Tunnel. *Terra Nova*, *31*(3), 281–294. https://doi.org/10.1111/ter.12398

Koulakov, I., Kaban, M. K., Tesauro, M., & Cloetingh, S. A. P. L. (2009). P-and S-velocity anomalies in the upper mantle beneath Europe from tomographic inversion of ISC data. *Geophysical Journal International*, *179*(1), 345–366. https://doi.org/10.1111/j.1365-246x.2009.04279.x

Krsnik, E., Methner, K., Campani, M., Botsyun, S., Mutz, S. G., Ehlers, T. A., et al. (2021). Miocene high elevation in the central Alps. *Solid Earth*, *12*(11), 2615–2631. https://doi.org/10.5194/se-12-2615-2021

Kuhlemann, J., Dunkl, I., Brügel, A., Spiegel, C., & Frisch, W. (2006). From source terrains of the Eastern Alps to the Molasse Basin: Detrital record of non-steady-state exhumation. *Tectonophysics*, *413*(3–4), 301–316. https://doi.org/10.1016/j.tecto.2005.11.007

Kummerow, J., Kind, R., Oncken, O., Giese, P., Ryberg, T., Wylegalla, K., et al. (2004). A natural and controlled source seismic profile through the Eastern Alps: TRANSALP. *Earth and Planetary Science Letters*, *225*(1–2), 115–129. https://doi.org/10.1016/j.epsl.2004.05.040

Kurz, W., Handler, R., & Bertoldi, C. (2008). Tracing the exhumation of the Eclogite zone (Tauern Window, Eastern Alps) by $^{40}Ar/^{39}Ar$ dating of white mica in eclogites. *Swiss Journal of Geosciences*, *101*(1), 191–206. https://doi.org/10.1007/s00015-008-1281-1

Lammerer, B., Gebrande, H., Lüschen, E., & Veselá, P. (2008). A crustal-scale cross-section through the Tauern Window (eastern Alps) from geophysical and geological data. *Geological Society, London, Special Publications*, *298*(1), 219–229. https://doi.org/10.1144/sp298.11

Lammerer, B., & Weger, M. (1998). Footwall uplift in an orogenic wedge: The Tauern Window in the Eastern Alps of Europe. *Tectonophysics*, *285*(3–4), 213–230. https://doi.org/10.1016/s0040-1951(97)00272-2

Le Breton, E., Brune, S., Ustaszewski, K., Zahirovic, S., Seton, M., & Müller, R. D. (2021). Kinematics and extent of the Piemont-Liguria Basin–implications for subduction processes in the Alps. *Solid Earth Discussions*, *12*(4), 1–42. https://doi.org/10.5194/se-12-885-2021

Linzer, H. G., Decker, K., Peresson, H., D'll'Mour, R., & Frisch, W. (2002). Balancing lateral orogenic float of the Eastern Alps. *Tectonophysics*, *354*(3–4), 211–237. https://doi.org/10.1016/s0040-1951(02)00337-2

Lippitsch, R. (2002). *Lithosphere and upper mantle P-wave velocity structure beneath the Alps by high-resolution teleseismic tomography* (Doctoral dissertation). ETH Zurich.

Lippitsch, R., Kissling, E., & Ansorge, J. (2003). Upper mantle structure beneath the Alpine orogen from high-resolution teleseismic tomography. *Journal of Geophysical Research*, *108*(B8), 2376. https://doi.org/10.1029/2002jb002016

Lock, J., & Willett, S. (2008). Low-temperature thermochronometric ages in fold-and-thrust belts. *Tectonophysics*, *456*(3–4), 147–162. https://doi.org/10.1016/j.tecto.2008.03.007

Lüschen, E., Borrini, D., Gebrande, H., Lammerer, B., Millahn, K., Neubauer, F., et al. (2006). TRANSALP—Deep crustal vibroseis and explosive seismic profiling in the Eastern Alps. *Tectonophysics*, *414*(1–4), 9–38. https://doi.org/10.1016/j.tecto.2005.10.014

Lüschen, E., Lammerer, B., Gebrande, H., Millahn, K., & Nicolich, R., & TRANSALP Working Group. (2004). Orogenic structure of the Eastern Alps, Europe, from TRANSALP deep seismic reflection profiling. *Tectonophysics*, *388*(1–4), 85–102. https://doi.org/10.1016/j.tecto.2004.07.024

McQuarrie, N., & Ehlers, T. A. (2015). Influence of thrust belt geometry and shortening rate on thermochronometer cooling ages: Insights from thermokinematic and erosion modeling of the Bhutan Himalaya. *Tectonics*, *34*(6), 1055–1079. https://doi.org/10.1002/2014tc003783

McQuarrie, N., & Ehlers, T. A. (2017). Techniques for understanding fold-thrust belt kinematics and thermal evolution. In *Linkages and feedbacks in orogenic process: A volume in honor of Robert D Hatcher Jr* (Vol. 213, pp. 25–54). Geological Society of America.

McQuarrie, N., Eizenhöfer, P. R., Long, S. P., Tobgay, T., Ehlers, T. A., Blythe, A. E., et al. (2019). The influence of foreland structures on hinterland Cooling: Evaluating the drivers of exhumation in the eastern Bhutan Himalaya. *Tectonics*, *38*(9), 3282–3310. Portico. https://doi.org/10.1029/2018tc005340

Mellere, D., Stefani, C., & Angevine, C. (2000). Polyphase tectonics through subsidence analysis: The Oligo-Miocene Venetian and Friuli Basin, North-East Italy. *Basin Research*, *12*(2), 159–182. https://doi.org/10.1046/j.1365-2117.2000.00120.x

Methner, K., Campani, M., Fiebig, J., Löffler, N., Kempf, O., & Mulch, A. (2020). Middle Miocene long-term continental temperature change in and out of pace with marine climate records. *Scientific Reports*, *10*(1), 1–10. https://doi.org/10.1038/s41598-020-64743-5

Mitterbauer, U., Behm, M., Brückl, E., Lippitsch, R., Guterch, A., Keller, G. R., et al. (2011). Shape and origin of the East-Alpine slab constrained by the ALPASS teleseismic model. *Tectonophysics*, *510*(1–2), 195–206. https://doi.org/10.1016/j.tecto.2011.07.001

Moratto, L., Romano, M. A., Laurenzano, G., Colombelli, S., Priolo, E., Zollo, A., et al. (2019). Source parameter analysis of microearthquakes recorded around the underground gas storage in the Montello-Collalto Area (Southeastern Alps, Italy). *Tectonophysics*, *762*, 159–168. https://doi.org/10.1016/j.tecto.2019.04.030

Most-Angelmaier, P. (2003). *Late Alpine cooling histories of tectonic blocks along the central part of the TRANSALP-Traverse (Inntal-Gadertal): Constraints from geochronology* (PhD thesis). Univ. Tübingen.

Müller, R. D., Zahirovic, S., Williams, S. E., Cannon, J., Seton, M., Bower, D. J., et al. (2019). A global plate model including lithospheric deformation along major rifts and orogens since the Triassic. *Tectonics*, *38*(6), 1884–1907. https://doi.org/10.1029/2018tc005462

Naylor, M., & Sinclair, H. D. (2007). Punctuated thrust deformation in the context of doubly vergent thrust wedges: Implications for the localization of uplift and exhumation. *Geology*, *35*(6), 559–562. https://doi.org/10.1130/g23448a.1

Naylor, M., Sinclair, H. D., Willett, S., & Cowie, P. A. (2005). A discrete element model for orogenesis and accretionary wedge growth. *Journal of Geophysical Research*, *110*(B12), B12403. https://doi.org/10.1029/2003jb002940

Neubauer, F., Genser, J., Kurz, W., & Wang, X. (1999). Exhumation of the Tauern window, Eastern Alps. *Physics and Chemistry of the Earth Part A: Solid Earth and Geodesy*, *24*(8), 675–680. https://doi.org/10.1016/s1464-1895(99)00098-8

Nocquet, J. M., & Calais, E. (2004). Geodetic measurements of crustal deformation in the Western Mediterranean and Europe. *Pure and Applied Geophysics*, *161*(3), 661–681. https://doi.org/10.1007/s00024-003-2468-z

Nussbaum, C. (2000). *Neogene tectonics and thermal maturity of sediments of the easternmost Southern Alps (Friuli area, Italy)* (p. 172) (PhD thesis). Univ. de Neuchâtel.

Ortner, H., Aichholzer, S., Zerlauth, M., Pilser, R., & Fügenschuh, B. (2015). Geometry, amount, and sequence of thrusting in the Subalpine Molasse of western Austria and southern Germany, European Alps. *Tectonics*, *34*(1), 1–30. https://doi.org/10.1002/2014tc003550

Ortner, H., Reiter, F., & Brandner, R. (2006). Kinematics of the Inntal shear zone–sub-Tauern ramp fault system and the interpretation of the TRANSALP seismic section, Eastern Alps, Austria. *Tectonophysics*, *414*(1–4), 241–258. https://doi.org/10.1016/j.tecto.2005.10.017

Paffrath, M., Friederich, W., & AlpArray and AlpArray-Swath D Working Group. (2021). Imaging structure and geometry of slabs in the greater Alpine area–A P-wave traveltime tomography using AlpArray Seismic Network data. In *Solid Earth discussions* (pp. 1–40).

Pfiffner, O. A. (2005). The Alps. In *Encyclopedia of geology* (Vol. 1, pp. 125–135). Elsevier.

Piromallo, C., & Morelli, A. (2003). P wave tomography of the mantle under the Alpine-Mediterranean area. *Journal of Geophysical Research*, *108*(B2). https://doi.org/10.1029/2002jb001757

Plomerová, J., Žlebčíková, H., Hetényi, G., Vecsey, L., & Babuška, V. (2022). Two subduction-related heterogeneities beneath the Eastern Alps and the Bohemian Massif imaged by high-resolution P-wave tomography. *Solid Earth*, *13*(1), 251–270. https://doi.org/10.5194/se-13-251-2022

Ratschbacher, L., Frisch, W., Linzer, H. G., & Merle, O. (1991b). Lateral extrusion in the Eastern Alps, part 2: Structural analysis. *Tectonics*, *10*(2), 257–271. https://doi.org/10.1029/90tc02623

Ratschbacher, L., Merle, O., Davy, P., & Cobbold, P. (1991). Lateral extrusion in the Eastern Alps, part 1: Boundary conditions and experiments scaled for gravity. *Tectonics*, *10*(2), 245–256. https://doi.org/10.1029/90tc02622

Reiners, P. W., Spell, T. L., Nicolescu, S., & Zanetti, K. A. (2004). Zircon (U-Th)/He thermochronometry: He diffusion and comparisons with $^{40}Ar/^{39}Ar$ dating. *Geochimica et Cosmochimica Acta*, *68*(8), 1857–1887. https://doi.org/10.1016/j.gca.2003.10.021

Rosenberg, C. L., Bellahsen, N., Rabaute, A., & Girault, J. B. (2021). Distribution, style, amount of collisional shortening, and their link to Barrovian metamorphism in the European Alps. *Earth-Science Reviews*, *222*, 103774. https://doi.org/10.1016/j.earscirev.2021.103774

Rosenberg, C. L., Berger, A., Bellahsen, N., & Bousquet, R. (2015). Relating orogen width to shortening, erosion, and exhumation during Alpine collision. *Tectonics*, *34*(6), 1306–1328. https://doi.org/10.1002/2014tc003736

Rosenberg, C. L., Schneider, S., Scharf, A., Bertrand, A., Hammerschmidt, K., Rabaute, A., & Brun, J. P. (2018). Relating collisional kinematics to exhumation processes in the Eastern Alps. *Earth-Science Reviews*, *176*, 311–344. https://doi.org/10.1016/j.earscirev.2017.10.013

Royden, L. H. (1993). The tectonic expression slab pull at continental convergent boundaries. *Tectonics*, *12*(2), 303–325. https://doi.org/10.1029/92tc02248

Scharf, A., Handy, M. R., Favaro, S., Schmid, S. M., & Bertrand, A. (2013). Modes of orogen-parallel stretching and extensional exhumation in response to microplate indentation and roll-back subduction (Tauern Window, Eastern Alps). *International Journal of Earth Sciences*, *102*(6), 1627–1654. https://doi.org/10.1007/s00531-013-0894-4

Schildgen, T. F., van der Beek, P. A., Sinclair, H. D., & Thiede, R. C. (2018). Spatial correlation bias in late-Cenozoic erosion histories derived from thermochronology. *Nature*, *559*(7712), 89–93. https://doi.org/10.1038/s41586-018-0260-6

Schlunegger, F., & Kissling, E. (2022). Slab load controls beneath the Alps on the source-to-sink sedimentary pathways in the Molasse basin. *Geosciences*, *12*(6), 226. https://doi.org/10.3390/geosciences12060226

Schlunegger, F., & Willett, S. (1999). Spatial and temporal variations in exhumation of the central Swiss Alps and implications for exhumation mechanisms. *Geological Society, London, Special Publications*, *154*(1), 157–179. https://doi.org/10.1144/gsl.sp.1999.154.01.07

Schmid, S. M., Fügenschuh, B., Kissling, E., & Schuster, R. (2004). Tectonic map and overall architecture of the Alpine orogen. *Eclogae Geologicae Helvetiae*, *97*(1), 93–117. https://doi.org/10.1007/s00015-004-1113-x

Schmid, S. M., Pfiffner, O. A., Froitzheim, N., Schönborn, G., & Kissling, E. (1996). Geophysical-geological transect and tectonic evolution of the Swiss-Italian Alps. *Tectonics*, *15*(5), 1036–1064. https://doi.org/10.1029/96tc00433

Schmid, S. M., Scharf, A., Handy, M. R., & Rosenberg, C. L. (2013). The Tauern Window (Eastern Alps, Austria): A new tectonic map, with cross-sections and a tectonometamorphic synthesis. *Swiss Journal of Geosciences*, *106*(1), 1–32. https://doi.org/10.1007/s00015-013-0123-y

Schneider, S., Hammerschmidt, K., Rosenberg, C. L., Gerdes, A., Frei, D., & Bertrand, A. (2015). U–Pb ages of apatite in the western Tauern Window (Eastern Alps): Tracing the onset of collision-related exhumation in the European plate. *Earth and Planetary Science Letters*, *418*, 53–65. https://doi.org/10.1016/j.epsl.2015.02.020

Schönborn, G. (1999). Balancing cross sections with kinematic constraints: The Dolomites (northern Italy). *Tectonics*, *18*(3), 527–545. https://doi.org/10.1029/1998tc900018

Serpelloni, E., Vannucci, G., Anderlini, L., & Bennett, R. A. (2016). Kinematics, seismotectonics and seismic potential of the eastern sector of the European Alps from GPS and seismic deformation data. *Tectonophysics*, *688*, 157–181. https://doi.org/10.1016/j.tecto.2016.09.026

Steenken, A., Siegesmund, S., Heinrichs, T., & Fügenschuh, B. (2002). Cooling and exhumation of the Rieserferner Pluton (Eastern Alps, Italy/Austria). *International Journal of Earth Sciences*, *91*(5), 799–817. https://doi.org/10.1007/s00531-002-0260-4

Stöckhert, B., Brix, M. R., Kleinschrodt, R., Hurford, A. J., & Wirth, R. (1999). Thermochronometry and microstructures of quartz—A comparison with experimental flow laws and predictions on the temperature of the brittle–plastic transition. *Journal of Structural Geology*, *21*(3), 351–369. https://doi.org/10.1016/s0191-8141(98)00114-x

Stockmal, G. S., Beaumont, C., Nguyen, M., Lee, B., & Sears, J. W. (2007). Mechanics of thin-skinned fold-and-thrust belts: Insights from numerical models. In *Special Papers Geological Society of America* (Vol. 433, p. 63).

Stolar, D. B., Willett, S. D., & Roe, G. H. (2006). Climatic and tectonic forcing of a critical orogen. In *Special Papers Geological Society of America* (Vol. 398, p. 241).

Storchak, D. A., Harris, J., Brown, L., Lieser, K., Shumba, B., Verney, R., et al. (2017). Rebuild of the Bulletin of the International Seismological Centre (ISC), part 1: 1964–1979. *Geoscience Letters*, *4*(1), 32. https://doi.org/10.1186/s40562-017-0098-z

Suppe, J. (1983). Geometry and kinematics of fault-bend folding. *American Journal of Science*, *283*(7), 684–721. https://doi.org/10.2475/ajs.283.7.684

Suppe, J. (1985). *Principles of structural geology*. Prentice Hall.

Tesauro, M., Kaban, M. K., & Cloetingh, S. A. (2009). A new thermal and rheological model of the European lithosphere. *Tectonophysics*, *476*(3–4), 478–495. https://doi.org/10.1016/j.tecto.2009.07.022

Thiede, R. C., & Ehlers, T. A. (2013). Large spatial and temporal variations in Himalayan denudation. *Earth and Planetary Science Letters*, *371–372*, 278–293. https://doi.org/10.1016/j.epsl.2013.03.004

Tomkin, J. H., & Roe, G. H. (2007). Climate and tectonic controls on glaciated critical-taper orogens. *Earth and Planetary Science Letters*, *262*(3–4), 385–397. https://doi.org/10.1016/j.epsl.2007.07.040

Trautwein, B., Dunkl, I., & Frisch, W. (2001). Accretionary history of the Rhenodanubian Flysch zone in the Eastern Alps–evidence from apatite fission-track geochronology. *International Journal of Earth Sciences*, *90*(3), 703–713. https://doi.org/10.1007/s005310000184

Ustaszewski, K., Schmid, S. M., Fügenschuh, B., Tischler, M., Kissling, E., & Spakman, W. (2008). A map-view restoration of the Alpine-Carpathian-Dinaridic system for the Early Miocene. *Swiss Journal of Geosciences*, *101*(S1), 273–294. https://doi.org/10.1007/s00015-008-1288-7

Vermeesch, P. (2009). RadialPlotter: A Java application for fission track, luminescence and other radial plots. *Radiation Measurements*, *44*(4), 409–410. https://doi.org/10.1016/j.radmeas.2009.05.003

Verwater, V. F., Le Breton, E., Handy, M. R., Picotti, V., Jozi Najafabadi, A., & Haberland, C. (2021). Neogene kinematics of the Giudicarie Belt and eastern Southern Alpine orogenic front (northern Italy). *Solid Earth*, *12*(6), 1309–1334. https://doi.org/10.5194/se-12-1309-2021

Vogt, K., Matenco, L., & Cloetingh, S. (2017). Crustal mechanics control the geometry of mountain belts. Insights from numerical modelling. *Earth and Planetary Science Letters*, *460*, 12–21. https://doi.org/10.1016/j.epsl.2016.11.016

von Blanckenburg, F., & Davies, J. H. (1995). Slab breakoff: A model for syncollisional magmatism and tectonics in the Alps. *Tectonics*, *14*(1), 120–131. https://doi.org/10.1029/94tc02051

Vosteen, H. D., Rath, V., Clauser, C., & Lammerer, B. (2003). The thermal regime of the Eastern Alps from inversion analyses along the TRANSALP profile. *Physics and Chemistry of the Earth, Parts A/B/C*, *28*(9–11), 393–405. https://doi.org/10.1016/s1474-7065(03)00060-3

Whipp, D. M., & Ehlers, T. A. (2019). Quantifying landslide frequency and sediment residence time in the Nepal Himalaya. *Science Advances*, *5*(4), eaav3482. https://doi.org/10.1126/sciadv.aav3482

Whipp, D. M., Ehlers, T. A., Braun, J., & Spath, C. D. (2009). Effects of exhumation kinematics and topographic evolution on detrital thermochronometer data. *Journal of Geophysical Research*, *114*(F4), F04021. https://doi.org/10.1029/2008JF001195

Whipple, K. X., & Meade, B. J. (2004). Controls on the strength of coupling among climate, erosion, and deformation in two-sided, frictional orogenic wedges at steady state. *Journal of Geophysical Research*, *109*(F1), F01011. https://doi.org/10.1029/2003jf000019

Willett, S., Beaumont, C., & Fullsack, P. (1993). Mechanical model for the tectonics of doubly vergent compressional orogens. *Geology*, *21*(4), 371–374. https://doi.org/10.1130/0091-7613(1993)021<0371:mmftto>2.3.co;2

Willett, S. D. (1999). Orogeny and orography: The effects of erosion on the structure of mountain belts. *Journal of Geophysical Research*, *104*(B12), 28957–28981. https://doi.org/10.1029/1999jb900248

Willett, S. D., & Brandon, M. T. (2002). On steady states in mountain belts. *Geology*, *30*(2), 175–178. https://doi.org/10.1130/0091-7613(2002)030<0175:ossimb>2.0.co;2

Willett, S. D., Herman, F., Fox, M., Stalder, N., Ehlers, T. A., Jiao, R., & Yang, R. (2020). Bias and error in modelling thermochronometric data: Resolving a potential increase in Plio-Pleistocene erosion rate. In *Earth surface dynamics discussions* (pp. 1–78).

Willingshofer, E., Sokoutis, D., Luth, S. W., Beekman, F., & Cloetingh, S. (2013). Subduction and deformation of the continental lithosphere in response to plate and crust-mantle coupling. *Geology*, *41*(12), 1239–1242. https://doi.org/10.1130/g34815.1

Wolff, R., Hetzel, R., Dunkl, I., & Anczkiewicz, A. A. (2021). New constraints on the exhumation history of the western Tauern Window (European Alps) from thermochronology, thermokinematic modeling, and topographic analysis. *International Journal of Earth Sciences*, *110*(8), 2955–2977. https://doi.org/10.1007/s00531-021-02094-w

Wölfler, A., Stüwe, K., Danišík, M., & Evans, N. J. (2012). Low temperature thermochronology in the Eastern Alps: Implications for structural and topographic evolution. *Tectonophysics*, *541*, 1–18. https://doi.org/10.1016/j.tecto.2012.03.016

Yamada, R., Matsuda, T., & Omura, K. (2007). Apatite and zircon fission-track dating from the Hirabayashi-NIED borehole, Nojima Fault, Japan: Evidence for anomalous heating in fracture zones. *Tectonophysics*, *443*(3–4), 153–160. https://doi.org/10.1016/j.tecto.2007.01.014

Zattin, M., Cuman, A., Fantoni, R., Martin, S., Scotti, P., & Stefani, C. (2006). From Middle Jurassic heating to Neogene cooling: The thermochronological evolution of the southern Alps. *Tectonophysics*, *414*(1–4), 191–202. https://doi.org/10.1016/j.tecto.2005.10.020

Zattin, M., Stefani, C., & Martin, S. (2003). Detrital fission-track analysis and sedimentary petrofacies as keys of alpine exhumation: The example of the Venetian Foreland (European Southern Alps, Italy). *Journal of Sedimentary Research*, *73*(6), 1051–1061. https://doi.org/10.1306/051403731051

Zhao, L., Paul, A., Malusà, M. G., Xu, X., Zheng, T., Solarino, S., et al. (2016). Continuity of the Alpine slab unraveled by high-resolution P wave tomography. *Journal of Geophysical Research: Solid Earth*, *121*(12), 8720–8737. https://doi.org/10.1002/2016jb013310